UNIVERSITÄT
BERN

OESCHGER CENTRE
CLIMATE CHANGE RESEARCH

Abrupt Climate Change in the Subpolar North Atlantic: Drivers and Impacts

Student:	Joas Müller, 21-117-841 Seidenweg 3, 3012 Bern
Supervisor:	Prof. Dr. Olivia Romppainen-Martius
Co-Supervisor:	Dr. Giuseppe Zappa
Co-Supervisor:	Dr. Alessio Bellucci

Date: July 4, 2023

1 Abstract

Recent studies utilizing the CMIP5 and CMIP6 model ensembles reveal that the subpolar North Atlantic (NA) is prone to deep convection collapsing leading to abrupt cooling of sea surface temperatures. Consequently, the latest comprehensive study on tipping points includes the subpolar gyre (SPG) deep convection on the list of core tipping elements of Earth's climate system. Here, we investigate the drivers and impacts of a collapse of deep convection in the subpolar NA and the role of internal variability using a coupled climate model large ensemble, namely CESM2-LENS. We identify the density anomaly at the surface resulting in the final cessation of deep mixing to be caused by the freshening of surface conditions. The ensemble shows abrupt cooling occurring approximately in 2045 with internal variability leading to a spread of $\pm$11 years. In each ensemble member, the subpolar NA transitions to a new state without deep convection, colder sea surface temperatures, and strongly reduced heat loss to the atmosphere. The changes in subpolar NA surface conditions impact the atmosphere and we identify significant shifts in the sea level pressure field and cooling of the Northern Hemisphere mean surface air temperature of around 0.4°C. The identification of abrupt cooling events caused by a convection collapse in the subpolar NA is sensitive to the choice of the reference region. Comparing different reference regions utilized in previous studies, we find the risk of abrupt cooling in the CMIP6 model ensemble to be underestimated. Internal variability does not determine if, but when abrupt cooling occurs, suggesting a forced response to larger-scale changes. We provide evidence for the collapse of deep convection being a component of a positive feedback mechanism resulting in the SPG circulation transitioning to a weaker state. Without deep convection at the center of the circulation, the density gradient-driven part of the gyre circulation vanishes and the circulation strength decreases by approximately 50 %. The tipping point of the subpolar NA is therefore reached decades prior to the abrupt cooling and abrupt cooling is an inevitable consequence of the tipping event. This points towards a potential misconception concerning drivers of abrupt climate change in the subpolar NA, connected tipping points, and their thresholds, highlighting the necessity for clarifying research efforts in the future.

Contents

2 Introduction

Abrupt climate change and so-called tipping elements in Earth's climate system introduce large uncertainties when predicting the evolution of our climate. To better understand when points of no return will be reached and to improve the skill of climate projections it is crucial to realistically represent these elements in climate models and understand how they might be linked (Lontzek et al., 2015; Wunderling et al., 2023). The most recent comprehensive study on tipping elements by Armstrong McKay et al. (2022) lists systems that are at risk of undergoing abrupt changes in the future. They include the subpolar North Atlantic as a region that is prone to change rapidly if certain warming thresholds are exceeded and term the Subpolar Gyre (SPG) a tipping element that is at risk to reach its tipping point even when keeping global mean temperatures below $1.5°C$, in line with the Paris agreement (Paris Agreement). This stresses the importance of understanding the drivers of SPG variability, the dynamics leading to abrupt changes of the subpolar North Atlantic climate, and the impact a new stable state of the SPG has on large-scale dynamics of the oceans and the atmosphere to improve climate model projections and our general understanding of the climate system.

Tipping Elements

Tipping elements are components of Earth's climate system that have more than one stable state (multistable regime) and can undergo a rapid transition from one into the other state if certain thresholds are reached. These thresholds are the system's tipping point and due to self-reinforcing feedbacks, the tipping element will changeover into another stable state, even when the forcing that pushed the system over its tipping point vanishes, resulting in abrupt climate change in the vicinity of the tipping element or even globally (Lenton et al., 2008; Steffen et al., 2018; Armstrong McKay et al., 2022). In the first comprehensive study on tipping elements, Lenton et al. (2008) identify large-scale components of the Earth's climate system that could reach a tipping point under continuous anthropogenic forcing. More recent studies have shown some tipping elements, such as the Greenland ice sheet or low-latitude coral reefs, might already have reached their tipping point and could not be kept in their initial stable state of the last millennia, even if immediate measures were taken (Armstrong McKay et al., 2022). Tipping elements introduce large uncertainty in future climate projections, due to the difficulty of correctly mimicking their behavior in climate models (Lontzek et al., 2015). Additionally, potential cascading effects, where one tipping elements transition into its new stable state results in other tipping elements reaching their tipping point, further contributes to the difficulty of correctly representing these systems in climate models (T. Liu et al., 2023; Swingedouw et al., 2020; Bathiany et al., 2018).

Before discussing what makes the SPG a tipping element, and the subpolar North Atlantic a region prone to show abrupt climate change in the future, we will discuss the drivers of SPG variability and its role in Earth's climate in the following section.

The Subpolar Gyre

The SPG is a cyclonic ocean circulation in the northern North Atlantic south of Greenland. SPG variability is linked to the North Atlantic Oscillation (NAO) on interannual to decadal time scales, with the positive (negative) NAO phase having a strengthening (weakening) effect on the circulation (Deshayes et al., 2008; Lohmann et al., 2009b; Delworth et al., 2016). One link between the NAO index and SPG strength is the amplified ocean heat flux to the atmosphere due to increased turbulent heat fluxes at the surface (Delworth et al., 2016; Lohmann et al., 2009a). Strong heat loss cools the water column and increases its density, which in turn strengthens the density gradient from the SPG border to its center. This increased density gradient leads to a stronger SPG circulation due to barotropic adjustment (Deshayes et al., 2008). The mean density of the water column directly reflects on the sea surface height (SSH). The SSH gradient from the circulations center to its edges is therefore a proxy for SPG strength and can be observed using satellite altimeters, improving and extending records of SPG size and strength (Foukal et al., 2017; Koul et al., 2020). Further, using SSH satellite altimeter records of the subpolar NA, Koul et al. (2020) present evidence for the SPG strength and size to modulate the amount of subpolar and subtropical water masses reaching the eastern subpolar NA.

Using the mixed layer depth (MLD) as a diagnostic quantity describing the strength of convection results in a more detailed description of the dynamic and thermodynamic drivers of SPG variability. Strong deep convection results in a deeper MLD, with the thickest MLD developing towards the end of the winter season when the preceding oceanic heat loss was strongest and temperatures reach their minimum. Using the Community Earth System Model version 1 (CESM1), Yeager et al. (2014) show the close connection between MLD and net surface buoyancy fluxes. Local heat and freshwater air–sea fluxes control the surface buoyancy fluxes, with the heat fluxes contributing to a significantly larger extent. They find the Labrador Sea (LS) to be the region where most of SPG deep convection occurs, with deep convection explaining most of the SPG variability. Therefore, great amounts of SPG variability can be explained by atmospheric conditions directly over the LS and early studies had already linked the MLD to the overall gyre transport (Böning et al., 2006; Yeager et al., 2014).

SSTs in the SPG are not only controlled by ocean-atmosphere heat fluxes and lateral advection of anomalously warm/cold waters, but additionally by deep convection activity. Strong deep convection (deep MLD) results in a thicker layer of water being

exposed to atmospheric conditions at the surface and vice versa. Hence, if convective activity is weak, only a shallow surface layer loses heat to the atmosphere. It is crucial to understand here that a shallower layer will experience amplified cooling due to the smaller body of water losing a similar amount of heat. However, the overall net heat loss of the water column is in turn smaller, due to the ocean-atmosphere temperature gradient at the surface being decreased (Beckmann, 2021). This explains why a thicker MLD is associated with a denser SPG core but not necessarily with colder SSTs.

Another feature of the subpolar NA is the negative trend of SSTs in some regions with the associated pattern often referred to as the "Warming Hole". This Warming Hole shows a negative temperature anomaly in the SPG that developed in recent decades (Ting et al., 2009; Drijfhout et al., 2012). Most of the excess heat in the atmosphere originating from global warming due to anthropogenic greenhouse gas emissions enters the oceans and thus leads to the rise of global SSTs (Levitus et al., 2012). Similar to the rise in surface air temperatures (SAT), the increase in SST is not uniform and differs regionally, with the largest deviation being the above-mentioned cooling of the subpolar NA or Warming Hole (Caesar et al., 2018; Drijfhout et al., 2012). Studies investigating the cooling of the subpolar NA using climate models came to different conclusions for the origin of the cold SST anomaly, mainly distinguishing between anomalously weak advection of warm water masses and the described effect of an overall decline in the MLD leading to colder than normal SSTs (Sgubin et al., 2017; Menary et al., 2018; Ghosh et al., 2023). This again highlights the large uncertainty inherent in climate models we observe in the future projections of the subpolar NA.

The Atlantic meridional overturning circulation (AMOC) is one of the most important elements of our climate system, with many studies pointing to the dangers of the AMOC approaching a tipping point and an ongoing debate on its drivers and impacts (Roquet et al., 2022; Caesar et al., 2018; Boers, 2021; Armstrong McKay et al., 2022). Additionally, a lot of work has been conducted on the close connection between SPG and AMOC. Böning et al. (2006) find that changes in the LS region and the overall SPG strength, resulting from changes in surface forcing associated with anomalous NAO conditions, can affect the AMOC at subtropical latitudes. Model studies find similar connections where NAO-like forcing influences LS density, the SPG strength, and with a lagged response the AMOC (Drijfhout et al., 2012; Gokhan Danabasoglu et al., 2019). These results are backed by the work of Yeager (2020) where they show how anomalous LS water thickness travels through internal pathways and accumulates close to the mid-Atlantic ridge. Here, these anomalies alter the zonal SSH gradient impacting the SPG and the AMOC. Additionally, strong links between changes in MLD and SST in the LS and the AMOC were found in a hindcast model configuration of CESM1 (Yeager et al., 2014). Thornalley et al. (2018) present evidence for the described atmosphere-ocean and SPG-AMOC interplay using paleoclimatic reconstructions. Furthermore, studies already suggest the presence of early warning signals for

a potential AMOC collapse using SPG SST as a proxy for AMOC stability (Boers, 2021).

SSTs in the NA are not only influenced by the atmosphere but also have an impact on large-scale atmospheric circulations and Europe's climate. The Atlantic Multidecadal Variability (AMV) describes a large-scale SST variability in the NA that has a great influence on atmospheric conditions (Ghosh et al., 2019). Zhang et al. (2016) determine the subpolar NA as the region showing the strongest low-frequency SST anomalies in the overall AMV and Hand (2020) finds a strong relationship between deep water formation in the LS and AMV. SSTs influence the atmosphere in two distinct ways. One is a linear response characterized by shallow atmospheric cooling due to colder SSTs, and the other is a transient eddy forced response where a strengthened SST gradient results in an increase in eddy activity close to the surface. This eddy activity propagates upwards and strengthens the Mid-Latitude Jet. These findings by Gervais et al. (2019) mainly focused on the North Atlantic Warming Hole which is commonly linked to an AMOC slowdown (Caesar et al., 2018), but a similar response to SST anomalies could be expected for SST anomalies in the SPG caused by a convection collapse. Further, studies have also linked anomalous SST conditions to extreme weather in Europe, emphasizing the role of the SPG not only for ocean dynamics but also for the atmosphere and Europe's climate (Duchez et al., 2016; Ghosh et al., 2019).

What makes the Subpolar Gyre a Tipping Element?

Armstrong McKay et al. (2022) term the SPG convection a tipping element mainly based on the findings by Sgubin et al. (2017) and Swingedouw et al. (2021). An alternative view on the subpolar NA and a possible tipping point like behavior is presented by taking the whole SPG circulation into account. Andreas Born et al. (2014) propose that the whole gyre circulation is in a bistable regime and the deep convection is an important component of this larger-scale tipping element. On the one hand, as Sgubin et al. (2017) and Swingedouw et al. (2021) show, the SPG is prone to a convection collapse resulting in a strong and rapid decline of SSTs. Here, a negative density anomaly develops at the surface resulting in an anomalously shallow MLD acting as a "lid" at the surface and hindering the deeper water masses to get in contact with the atmosphere. Therefore, the abrupt cooling of SSTs and a weakening of the SPG core's density resulting in a decline of SSH gradients and gyre circulation is the consequence. On the other hand, a weakening of the SPG strength and weaker boundary currents will dampen the advection of saline and dense waters from the gyre border towards the convection sites in the gyre center due to reduced mesoscale eddy activity. This decline in advection of more saline and dense waters to the gyre center will again start the chain of events resulting in a MLD decline, a less dense gyre core and a relaxation of SSH gradients ultimately

resulting in an even weaker SPG circulation (Andreas Born et al., 2014). This positive feedback mechanism leads to the bistable regime of the SPG and the possibility of abrupt changes in the subpolar NA if the system's tipping point and the corresponding threshold is reached. Additionally, A. Born et al. (2010) show the potential contribution of the current strong SPG circulation state to the stability of the Holocene climate. This stabilizing effect started approximately 8200 years ago when the SPG circulation transitioned from a weak state to the strong circulation state including the enhancement of deep convection in the LS. This again emphasizes the potential role the SPG plays in our climate system.
Assessing the risk of abrupt cooling events associated with a convection collapse in the SPG using the climate model ensembles of the Coupled Model Intercomparison Projects 5 and 6 (CMIP5/CMIP6), Sgubin et al. (2017) and Swingedouw et al. (2021) find only a few model realizations showing convection collapse and abrupt SST cooling events. Still, it is worth noting that models with higher skill in simulating the SPG stratification comprise convection collapse events in 45.5% (CMIP5) / 36.4% (CMIP6) of model initialization respectively. This implies that such events cannot be ruled out and are about as likely as not to occur in this century with Armstrong McKay et al. (2022) even concluding that the tipping point for the LS deep convection will be reached already in the coming decade.

Single model initial-condition large ensembles (SMILEs)

Single model initial-condition large ensembles (SMILEs) have many advantages mainly due to the big number of model initializations with slight variations in their initial conditions, increasing the sample size which in turn generally improves the statistical power of the analysis. One of the most important advantages is the possibility to distinguish between the natural variability of the model's climate system and the effects external forcings have on it. Additionally, SMILEs can be useful when studying extreme events with large return periods (Deser et al., 2020; Maher et al., 2021). Although tipping elements have a distinct underlying dynamic behavior compared to extreme events, studying these tipping points using SMILEs will bring new insights and improve the assessment of the risk of reaching a threshold that would result in abrupt climate changes. Due to the combination of internal variability and external forcing on the tipping elements, it remains difficult to predict tipping points and extending the analysis and research done on the most crucial tipping elements using SMILEs is urgently needed (Swingedouw et al., 2020).
To the best of our knowledge, assessing the SPG's potential of showing abrupt changes or a collapse of deep convection using a SMILE fully coupled climate model has not been done before.

Knowledge Gaps

Due to model biases and a temporal and spatial lack of records, the exact physical dynamics behind the SPG and AMOC are not yet fully understood and require further research to improve the understanding of their drivers. Assessing the proximity to their corresponding tipping points is crucial to understanding where global warming thresholds lie that would trigger irreversible changes in our climate system (W. Liu et al., 2017; Lozier et al., 2019). W. Liu et al. (2017) for example show that most climate models contain a bias towards a too-stable AMOC. A tipping point in the real-world climate system would hence be reached earlier than the models suggest. Other studies however mention the ongoing lag of records and uncertainty of AMOC projections (Roquet et al., 2022).
Swingedouw et al. (2021) reveal a big model uncertainty in the subpolar NA over the CMIP6 models when it comes to abrupt cooling in the region, not only for different models but also for different forcing scenarios. With the described complex feedback mechanisms involved in the SPG variability, different underlying drivers of deep convection collapse might be identified in different climate models. Therefore, different processes could result in the abrupt cooling and tipping of the SPG. This questions the robustness of the risk assessment made for reaching the subpolar NA's tipping point (Sgubin et al., 2017; Swingedouw et al., 2021; Armstrong McKay et al., 2022). Therefore using multiple model initializations of one single climate model will help to improve the risk assessment of a collapse of deep convection in the SPG and how it depends on different forcing scenarios.
It is further of great importance to study the consequences implied by abrupt changes in the SPG. Again, the intercomparison between different climate models introduces more uncertainty on how the general circulation models of the coupled climate models react to the anomalously cold SST patterns caused by a convection collapse.
What is not necessarily clear in many studies on abrupt changes in the subpolar NA is whether changes in the SPG strength always precede the anomalous surface conditions leading to the sea surface density anomaly that hinders deep convection, or if a deep convection collapse can be the initial event starting a decline in SPG strength (Lenton, 2012; Sgubin et al., 2017; Swingedouw et al., 2021). Armstrong McKay et al. (2022) estimate the threshold for the convection collapse as the tipping point. But as described earlier, other studies identify the deep convection at the gyre's center as a core element of a positive feedback loop that underlies the SPG circulation's bistable regime. Hence, the question arises whether the assessment made by Armstrong McKay et al. (2022) is accurate, or if the actual tipping point lies somewhere else.

Objectives

The overarching goal of this study is to improve the understanding of drivers of collapse of deep convection in the SPG and the corresponding abrupt climate change.
Taking advantage of the CESM2 (see Section 3) in its SMILE configuration namely the CESM2-LENS, we are going to identify convection collapse events in the SPG for a large number of model realizations to assess the timing and duration of the abrupt drops in SSTs, preceding oceanic conditions and drivers causing the collapse of deep convection, and the impact of the developing cold SST anomaly on atmospheric conditions.

The Objectives of this study are therefore as follows:

- Identify tipping events in CESM2-LENS and assess the model spread in the timing of their emergence.
- Assess how the timing of the abrupt changes is altered for different forcing scenarios.
- Determine what is driving deep convection collapse in CESM2 and investigate whether the cessation of deep convection in the SPG is a tipping element of its own, or a consequence of other large scale changes.
- Analyse the evolution of the ocean and atmosphere in proximity of the abrupt cooling events associated with a convection collapse in the SPG to understand the impacts on the climate system.
- Evaluate if the changes in the study designs between the work of Sgubin et al. (2017) and Swingedouw et al. (2021) influence the estimated decreased risk of abrupt cooling events in CMIP6 compared to CMIP5.

3 Data & Methods

The CESM2 Large Ensemble

A complete and long-lasting deep convection collapse has not been observed and we cannot use real-world data to study this phenomenon. We therefore rely on climate models that simulate the evolution of our climate system. These models are computer-based tools that help us understand how certain components of Earth's climate interact and change if external forcing is altered. Climate models use the fundamental physical equations governing the interactions and general behavior of the atmosphere and oceans. They therefore can represent the dynamical behavior of the climate system and help us to understand how climate and certain elements of the climate system might change under continuous greenhouse gas forcing. Hence, due to the lack of observations, climate models are the best tool to investigate the subpolar NA in regard to abrupt and large-scale changes connected to reaching its tipping point.

The main data set we are using for our study is CESM2 in its SMILE version (CESM2-LENS) consisting of 100 members (G. Danabasoglu et al., 2020; Rodgers et al., 2021). Swingedouw et al. (2021) already identified abrupt cooling events in two CESM2 CMIP6 model runs. This result, combined with the CESM models showing abrupt cooling events in the subpolar NA even in earlier versions and a good skill in resolving ocean stratification, makes CESM2-LENS a well-suited SMILE to study abrupt cooling in the SPG (Sgubin et al., 2017; Swingedouw et al., 2021).
The atmosphere and ocean components of CESM2 are the Community Atmosphere Model version 6 (CAM6) and the Parallel Ocean Program Version 2 (POP2) (G. Danabasoglu et al., 2020; Smith et al., 2010). CAM6 has a spatial resolution of $1.25°/0.9°$ in longitude/latitude and 32 vertical levels. POP2 has a uniform resolution in the zonal direction of $1.125°$ and a variable resolution in the meridional direction with a finer resolution closer to the Equator and a nominal resolution of $1°$. In the vertical POP2 has 60 layers, with the top 200 m consisting of 20 layers and the remaining deeper ocean consisting of 40 layers. It is important to note that this relatively coarse resolution of POP2 requires mesoscale eddies to be parameterized.
CESM2-LENS simulates the period from 1850 to 2100. 1850 to 2015 represents the historical data set that is forced by the already observed changes in greenhouse gas and aerosol concentrations and land-use changes. From 2015 to 2100 CESM2-LENS is forced by the Shared Socioeconomic Pathway 3 (SSP370) which results in an additional radiative forcing of 7 $\frac{W}{m^2}$ by the end of this century.
To create ensemble spread, crucial for the correct representation of internal variability, the initial states of each ensemble member are altered using different combinations of oceanic and atmospheric initial states. 20 ensemble members use different years of the

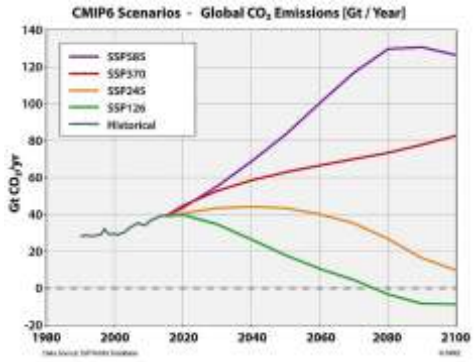

(a) Global CO_2 emissions depending on the SSP forcing scenario.

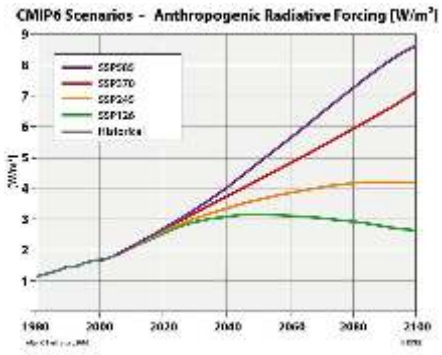

(b) Anthropogenic Radiative Forcing depending on the SSP forcing scenario.

Figure 1: Figures from Böttinger et al. (2020) showing the evolution of future CO_2 emissions and the resulting changes in radiative forcing depending on the forcing scenario.

preindustrial CESM2 control run as their initial conditions. The chosen years are 1001 to 1191 with 10 years difference between each initial condition. The remaining 80 members start from four substantially different AMOC states identified in the years 1231, 1251, 1281, and 1301 of the preindustrial control run. For each of the four AMOC states, 20 random perturbations of the atmospheric potential temperature field are used to result in the desired ensemble spread.
Additionally to CESM2-LENS, we use data from nine CMIP6 CESM2 runs. The CMIP6 CESM2 runs are forced by SSP126, SSP370, and SSP585 (three runs for each scenario) resulting in an additional radiative forcing by year the 2100 of 2.6 $\frac{W}{m^2}$, 7.0 $\frac{W}{m^2}$, and 8.5 $\frac{W}{m^2}$ respectively (Meinshausen et al., 2020). The differences between the scenarios emissions and radiative forcing evolution can be seen in Figure 1.

It is crucial to understand how close we are to the described tipping point to understand when we force this key element of our climate system into a new stable state. Using different forcing scenarios enables us to assess how the risk and timing of a collapse of SPG deep convection vary for different forcing scenarios.

SPG Reference Region

To investigate abrupt cooling in the subpolar NA related to a collapse of deep convection, a reference region needs to be determined for which the surface conditions are analyzed. Sgubin et al. (2017) applied a complex method using SST trends involving all models and forcing scenarios of the CMIP5 model ensemble to determine their reference region (Fig.

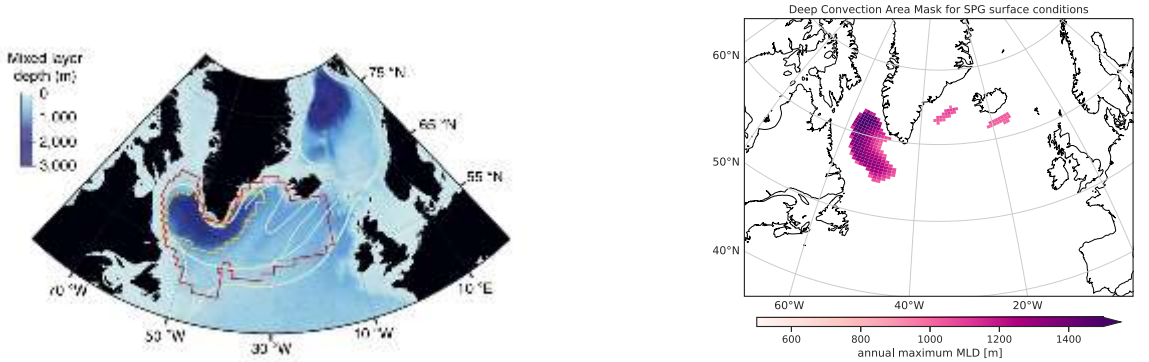

(a) Figure from Sgubin et al. (2017) showing MLD reanalysis data from GLORYS over the period 1993-2012. Red contour shows SPG area for the SST-trend approach that Sgubin et al. (2017) used to define their reference region, Yellow contour shows SPG region defined by the MLD being greater than 1000 m in the annual maximum of the reanalysis data used for sensitivity testing, with no significant differences in the results found.

(b) Ensemble and time mean (1850-1950) of annual maximum MLD, only showing the regions where the threshold of 1000 m is exceeded and therefore represents the mask to analyse SPG conditions for abrupt cooling events.

Figure 2: Masking subpolar NA to analyze SPG properties relating to abrupt cooling events.

2a Red contour). As a sensitivity test, they additionally mask the reference region using a threshold for mean annual-maximum MLD (2a Yellow contour), with no significant changes in the results. To minimize the risk of detecting SST signals not linked to changes in the strength of deep convection, we make use of the second approach in our study and additionally test whether taking a larger reference region changes the results. Therefore, we will apply the proposed threshold of 1000 m in the annual maximum MLD to mask the SPG reference region (Sgubin et al., 2017).

The resulting mask can be seen in Figure 2b. The main region of deep convection in CESM2 is the Labrador Sea (LS) located southwest of Greenland. Additionally, a small part of the Irminger Sea between Iceland and Greenland and a small region south of Iceland show also moderate deep convection exceeding the threshold of 1000 m in annual maximum MLD. When observing the two maps of deep convection in Figure 2, we find CESM2 to locate the region where deep convection occurs well and in line with the CMIP5 model ensemble and reanalysis data, justifying the choice of using CESM2 in our work. Hence, when analyzing SPG conditions in light of a potential collapse of deep convection and the consequent abrupt cooling events, we focus on this masked region. Quantities like SST, SSS, and MLD are analyzed using the area-weighted average value of the SPG mask.

Identification of Abrupt Cooling Events

To identify abrupt cooling events, Sgubin et al. (2017) use the pre-industrial control simulations to estimate the internal unforced variability of the SST averaged over the predefined region (SPG SST). The SPG SST rate of change time series is now computed using an 11-year window. Therefore, the rate of change at a given time step is the SST difference between two time steps separated by 11 years (Eq.1). After scaling this rate of change time series, an abrupt cooling event is termed as such when the normalized SPG SST rate of change drops below 3. This corresponds to an event with a likelihood of occurrence of 0.3 % under a Gaussian assumption and unforced conditions.
In our study we will make use of the same approach and stay consistent to allow a comparison of our findings with the mentioned work of Sgubin et al. (2017) and Swingedouw et al. (2021). The only difference is that we use the historical data from 1850 to 1900 instead of the preindustrial control simulation to scale the time series.

SPG SST 11 year rate of change time series:

$$\mathrm{SST\_11\_roc}_t = \mathrm{SST}_{t+5} - \mathrm{SST}_{t-5} \tag{1}$$

Variables and Indices

SPG strength

To define the SPG strength we use the barotropic streamfunction (BSF) data which is a diagnostic quantity in CESM2. It is defined as the depth-integrated volume transport $v(x, y, z)$ and is dependent on longitude and latitude (Eq. 2).

$$\Psi(x, y) = \int_0^{z_{\mathrm{bottom}}} v(x, y, z)\, dz \tag{2}$$

With the SPG circulation being cyclonic and therefore appearing as a depression in the BSF data, we define the SPG strength as the absolute value of the minimum BSF data in a box that always contains the minimum of the BSF in the subpolar NA. Reproducing the SPG strength index is not sensitive to the exact box size as long as the minimum of the BSF is enclosed at any given time.

$$\text{SPG strength} = |\min(\psi(x, y))| \tag{3}$$

Table 1: Table showing all variables used in our study, including their exact names in CESM2, units, time averaging periods, and description.

Variable Name	Unit	Time Averaging	CESM2 Name	Description
SST	[°C]	monthly	SST	Sea Surface Temperature
MLD	[m]	monthly	HMXL	Mixed-Layer Depth
SSS	[psu]	monthly	SSS	Sea Surface Salinity
BSF	[Sv]	monthly	BSF	Barotropic Streamfunction
MOC	[Sv]	monthly	MOC	Meridional Overturning Circulation
PSL	[hPa]	monthly	PSL	Sea Level Pressure
SAT	[°C]	monthly	TS	Surface Air Temperature
PRECIP	[mm/day]	monthly	PRECT	Total Precipitation
SHF	[W/m^2]	monthly	SHF	Surface Heat Flux

AMOC strength

The zonally averaged streamfunction $\psi(y, z)$ (Eq. 4) is the commonly used quantity to assess the meridional overturning circulation (MOC) in the ocean. The AMOC is therefore defined similar to Equation 2, with the difference that it is integrated from the western to the eastern boundary (zonal average) of the Atlantic Ocean.

$$\psi(y, z) = \int v(x, y, z) dx \tag{4}$$

We now define AMOC strength as the maximum of $\psi(y, z)$ from 26.5° N - 60° N and 500 m of depth to the ocean bottom (Eq. 5).

$$\text{AMOC strength} = \max_{\substack{500\,\text{m} \leq z \leq \text{ocean bottom} \\ 26.5°\text{N} \leq y \leq 60°\text{N}}} \psi(y, z) \tag{5}$$

4 Evolution of the Subpolar North Atlantic

Subpolar Gyre SST and MLD Evolution

The evolution of SPG SST and MLD depicted in Figure 3 clearly showcases the described abrupt changes in the subpolar NA.
We find a gradual increase in SPG SST in the historical data reaching a maximum shortly after the year 2000 when analyzing the ensemble mean. In the following years, until approximately 2040, SPG SST decreases and shows a negative trend, only slightly stronger in magnitude than the preceding positive trend. From 2040 to 2060, the negative trend in the ensemble mean SST increases leading to a steep drop of more than 2°C in 20 years. When comparing with the single ensemble member (dashed blue line Fig.3), we attribute this amplified negative trend in the ensemble mean to the abrupt cooling of each ensemble member during this period. The actual abruptness of SPG cooling becomes visible for the plotted single ensemble member where the drop exceeds 3°C in one year. The increase in ensemble variance from 2040 to 2060 that is perceptible in the distribution of the single members (thin blue lines) illustrates the spread in the exact year in which the abrupt cooling events occur in each member. From 2060 to 2100, the SPG SST increases again at a rate bigger than what we observe in the historical data.

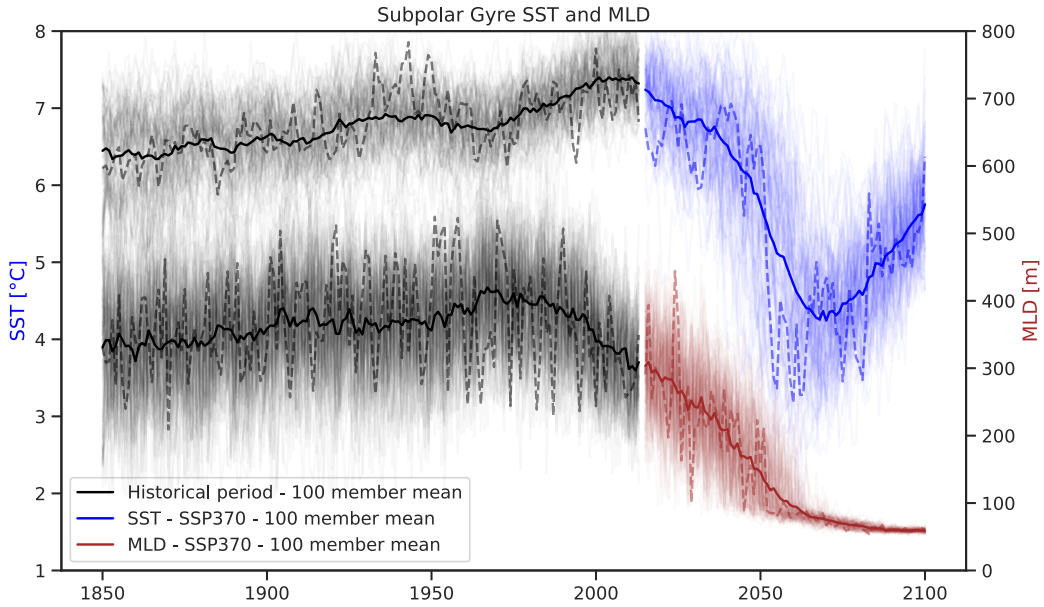

Figure 3: Annual SPG SST (blue) and MLD (red) from 1850 - 2100 for each ensemble member (thin lines) and ensemble means (thick lines). Dashed lines show a single ensemble member (member '1001.001').

The SPG MLD shows a positive trend from 1850 to around 1970 where it increases from 300 m to 400 m in the ensemble mean. After 1980 the MLD decreases steadily and falls below 100 m around 2060. From this point onwards the MLD does not recover and the strong MLD variance we identify in the historical data slowly decreases during the overall decline until 2060 and almost completely vanishes afterward in relation to the variance of the preceding years (Fig.3 and Appendix Fig.27).
When comparing the two time series of SST and MLD, we find that although the abrupt cooling is caused by a collapse of deep convection and therefore a strong decline in the MLD, the abruptness of the event is apparent only in the SST time series. This is even more pronounced when comparing the dashed time series corresponding to the single member. In relation to the abrupt SST drop in 2050 (dashed blue line), we find large and abrupt MLD changes cooccurring with small SST changes in the historical period. Considering this, the MLD decline corresponding to the abrupt cooling event is smaller in magnitude than many strong anomalies in MLD in the historical data. This suggests the gradual decline in the SPG MLD starting in the 1980s to be relevant for abrupt cooling events in the subpolar NA. In other words, the collapse of deep convection leading to the abrupt decrease in SST is a slow process and sets in decades before the discussed events.

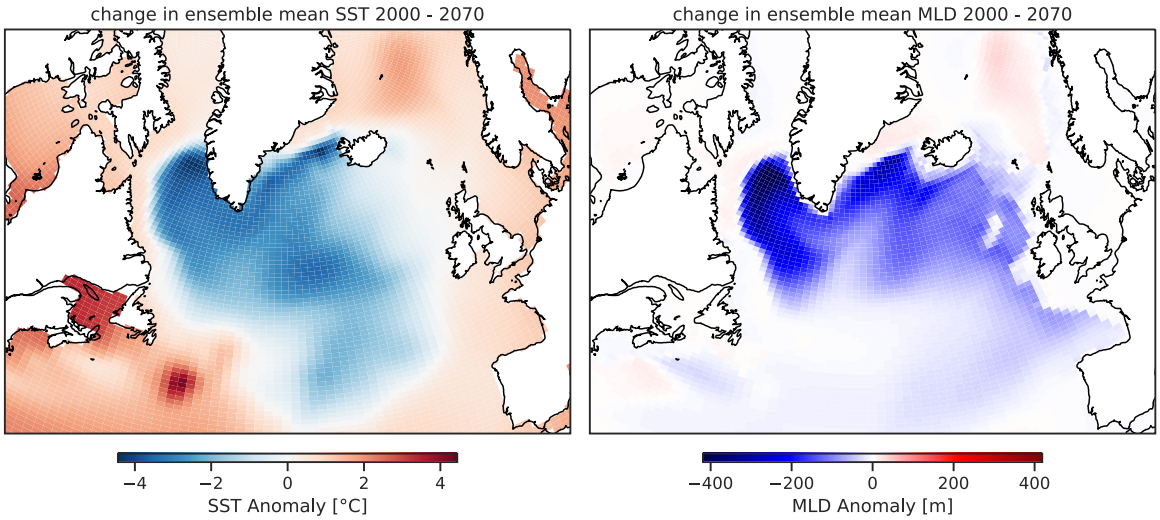

Figure 4: Spatial pattern of SST and MLD anomalies in 2070 after the abrupt cooling of the whole large ensemble (see Fig.3). Anomalies in respect to 1990-2000 climatology.

The SST and MLD anomalies that emerge during the period of abrupt cooling in the subpolar NA are shown in Figure 4. We find that not only for the region with strong deep convection masked for the time series previously discussed (Fig. 2 & 3), but for the whole SPG and bordering regions a negative SST anomaly of up to -4° C develops.

Outside of the SPG, SSTs have increased most likely due to the mentioned direct effect of global mean temperature rise and corresponding oceanic heat uptake.
We identify the strongest MLD anomalies of up to -400 m in the LS and Irminger Sea. Here, the anomalous patterns of MLD and SST match well. Differences between the two can be seen in the extent of the negative MLD anomaly extending further towards Europe and the Iceland-Scotland ridge. Apart from a small increase in MLD in the Nordic Seas and off the coast of North America, the NA shows a large-scale decline in MLD (Fig.4).
These results showcase that in CESM2-LENS all ensemble members show a change towards a state without deep convection in the subpolar NA. This causes the observed decline in SSTs in regions where the convective activity contributes significantly to the surface temperatures (see Section 2). After the new state without deep convection is reached, SSTs increase again, but the MLD does not show any signs of recovery and stays in the new low variability and shallow state.

Abrupt Cooling Event Identification

Using the proposed method (Section 3), we detect that all ensemble members except 3 show abrupt cooling. The ensemble mean year of abrupt SPG cooling is detected in 2045 $\pm$11 years (Fig. 5, upper panel). Visually comparing this result with the underlying SST data in Figure 5, we find this method to detect the abrupt changes well.
The SPG SST shows a more prominent abrupt change compared to the SPG MLD where the rarity of the event is not visible in the magnitude of the abrupt change, but rather the total decrease below a MLD threshold for many consecutive years that is unprecedented in the historical time series (Fig.3). However, for identifying the end of the abrupt changes, using the MLD time series is more suitable than using the SST. With the vanishing deep mixing, the warming effect of convection on SST disappears (see Section 2). In turn, SSTs are driven to a larger extent by the advection of warmer or colder water masses and by the direct warming and cooling effect of the atmosphere. Hence, the SPG SST development towards the end of the abrupt changes and the decades afterward is likely dependent on the forcing scenario.
Therefore, to further investigate the time scales of convection collapse events in the SPG, we define another detection method that indicates the end of a convection collapse event using the MLD. After our first analysis of the MLD evolution, we find the abrupt changes to result in a completely collapsed state of deep convection with strongly decreased variability and small ensemble spread compared to the historical data. We observe that all ensemble members show the complete collapse of MLD towards a new stable state with strongly decreased variability and MLD values below 100 m (Fig.3). The MLD is therefore a suitable quantity to determine when the transition towards the collapsed state took place and the new state without convection is reached. We define

the end of the convection collapse as the point in time where SPG MLD is below 100 m and does not reach a value larger than 100 m until the end of the simulation.

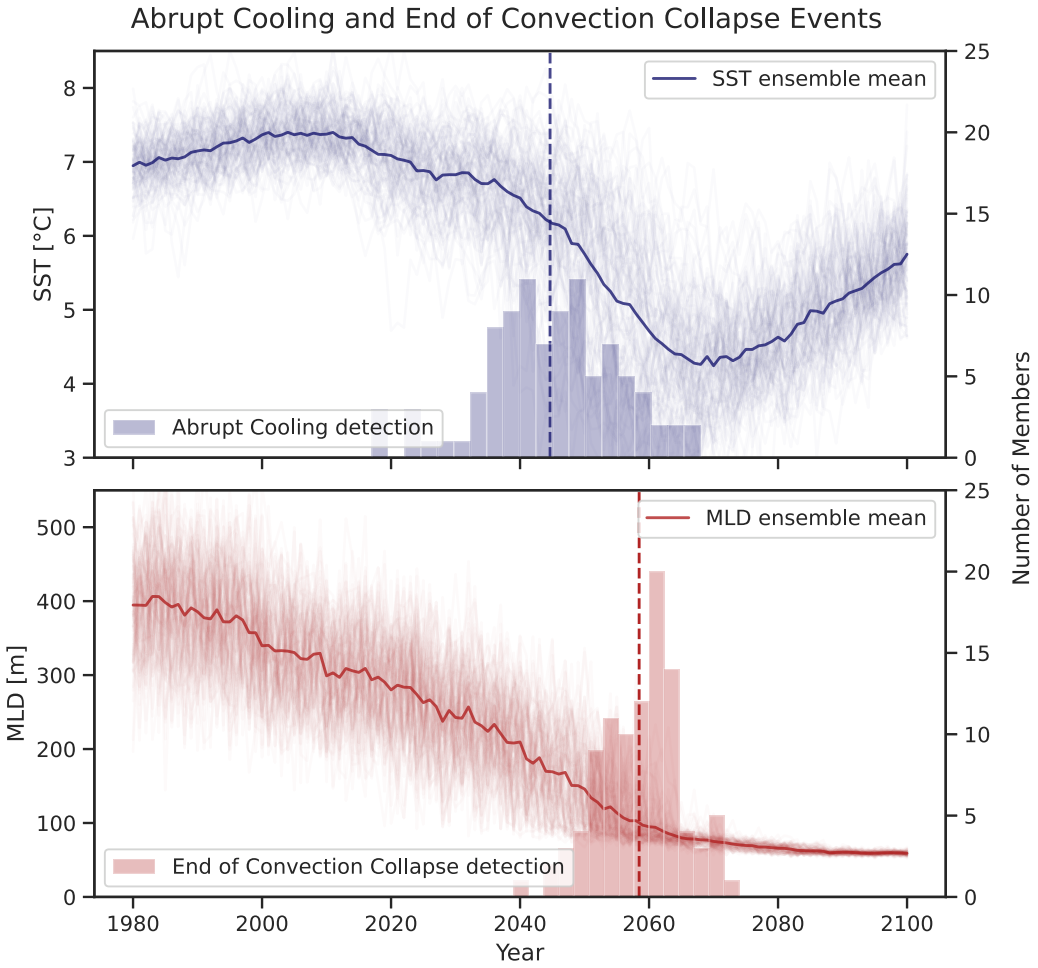

Figure 5: SST and MLD data as in Figure 3. Blue histogram shows the detection of an abrupt cooling event using the 11-year SST rate of change time series (see Section 3 ; shown is the original SST time series). Red histogram shows the years where the end of tipping is detected using the MLD time series and the in section 3 described method.

This supplementary method of using the MLD time series to identify the end of the convection collapse results in the ensemble mean end of collapse to be detected in 2058 ±6 years. Visually testing this result with the underlying MLD in Figure 5 makes us conclude that this method detects the ensemble mean end of the abrupt changes well. We now can identify the duration of the convection collapse events using the period from the first detection of a strongly anomalous SPG SST rate of change to the described collapsed state of deep convection. The result is 13 years (2045 - 2058) in

the ensemble mean. Noteworthy is a rather large spread with some members showing shorter collapse event periods below 5 years and some members indicating the collapse of deep convection happening over a period of almost 40 years (Fig.6).

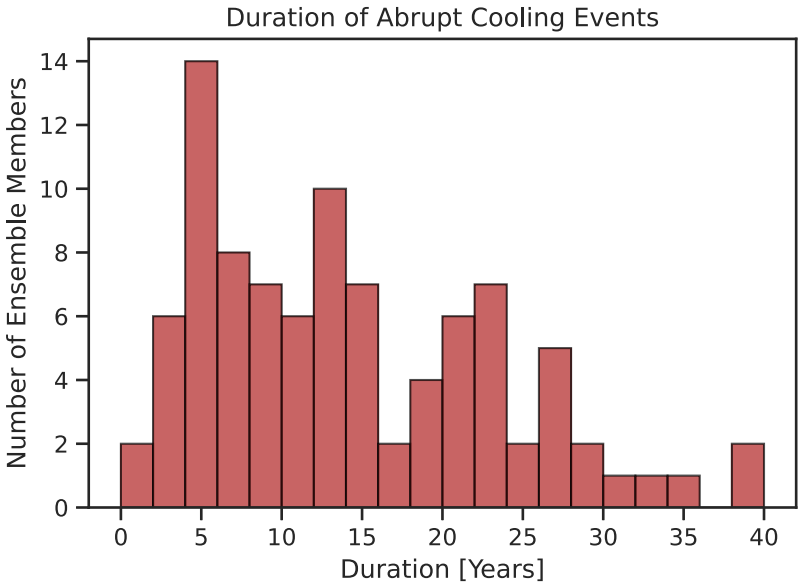

Figure 6: Histogram showing the duration from the detection of the the abrupt cooling to the detection of the end of the convection collapse. In other words: Duration from the first signal of very anomalous SPG SST drop to the SPG MLD falling below the threshold value permanently (See Fig.5).

These results suggest that although the MLD decline and the complete collapse of deep convection is likely to cause the abrupt cooling of the subpolar NA, other drivers of SSTs remain important and may prevent or dampen an immediate abrupt and strong cooling. This emphasizes the role of internal variability in influencing the decline of SST following a collapse of convection.
The detection method provides us with good results that are comparable with previous work. But we have to note that the method is not flawless. Using the MLD, we find that all ensemble members show a collapse of deep convection. But the SST of three ensemble members does not decline rapidly enough to trigger the detection threshold. Additionally, we find one ensemble member that shows a strong enough decline in SST, but only after the MLD already collapsed. These members were excluded from above described analysis and Figures 5 and 6.

Dependence on Research Area

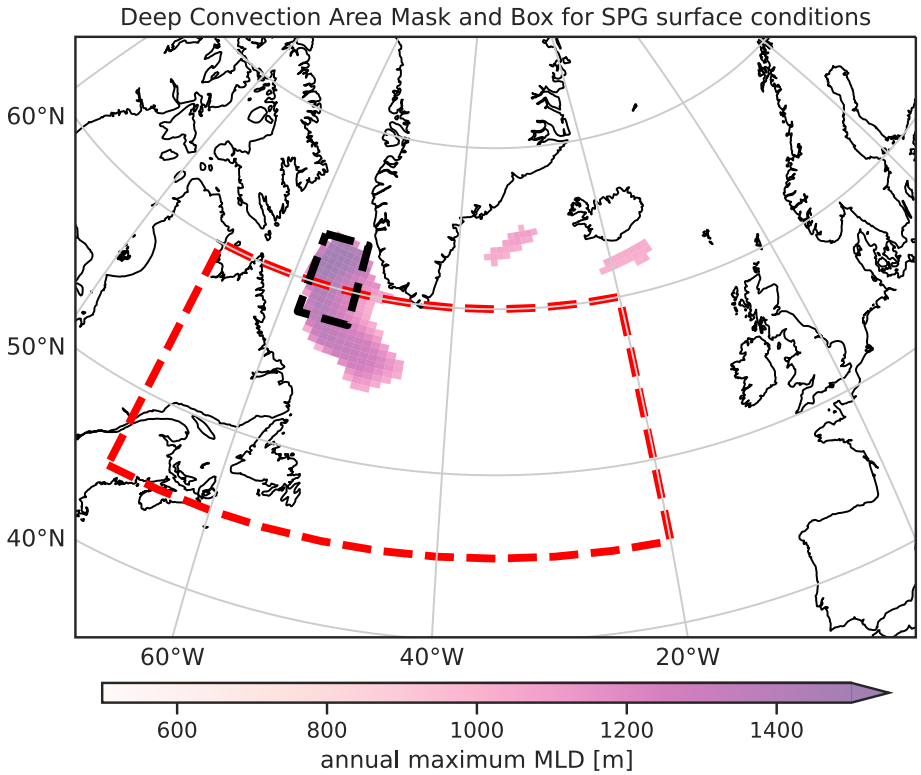

Figure 7: Map showing the applied SPG mask defined using the annual maximum MLD exceeding 1000 m (purple shading) and two boxes for the identification of abrupt cooling using SAT. Red box represents the whole subpolar NA as in Swingedouw et al. (2021) and black box is placed directly over the main deep convection site in the LS excluding regions not affected by strong changes in the convective activity.

Sgubin et al. (2017) use the CMIP5 and Swingedouw et al. (2021) the CMIP6 model ensemble to assess the risk of abrupt cooling in the subpolar NA. They apply the same identification method for detecting the abrupt cooling events but change the variable and reference region from the first to the second study. In the first study, a mask is defined using the model ensemble SSTs (Fig.2, red mask). For the abrupt cooling identification, the SPG SST (average SST of the masked region) is used. In the second study, SAT is utilized and the research area is defined as the box from 45°- 60° N and 20°- 70° W (Fig.7, red box). SST and SAT are highly correlated and using SAT instead of SST is unlikely to change the results. But with the red box in Figure 7 only covering approximately half of the deep convection area masked for our study, the question emerges whether this difference has a significant impact on the result. We therefore

compare how the detection of abrupt cooling is affected by this change in the reference region. Additionally, we include a third reference region. This third box (Fig.7, black box from 58°- 63° N and 52°- 58° W) is placed directly over the north-eastern part of the LS where convection is strongest and the SAT inside this box is averaged to compare the resulting time series with our SPG SST time series and the SAT time series of the red box.

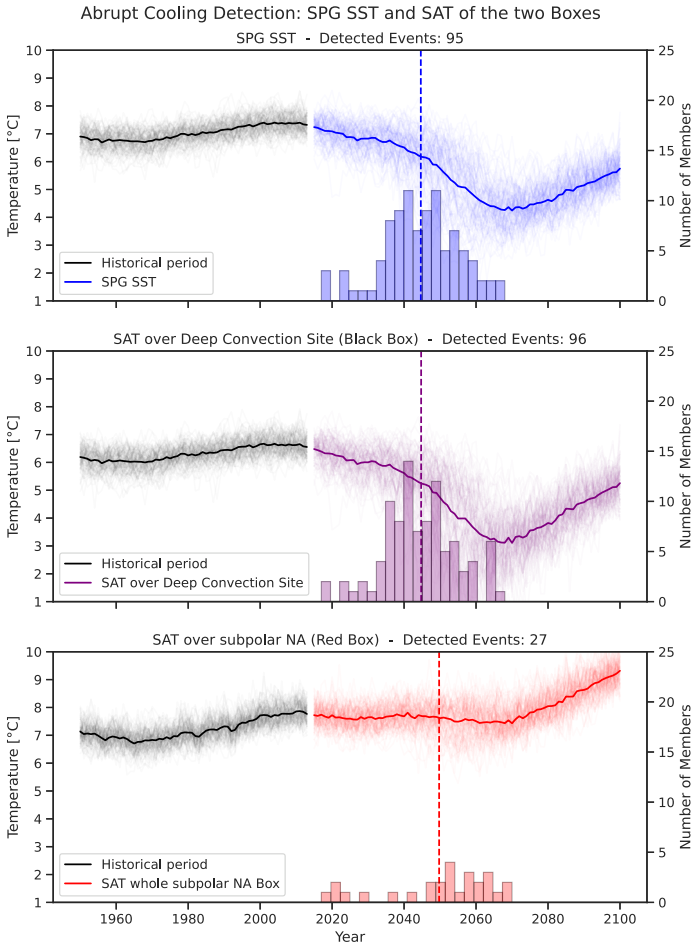

Figure 8: Identification of abrupt cooling events for three different temperature time series in the subpolar NA region. Thick lines are the ensemble mean, thin lines are the single members, histograms indicate the number of detected events for each year, vertical dashed lines indicate the ensemble mean year of detection. Upper panel is the SPG SST as already shown in Figure 5 (blue), middle/lower panel shows the result for using the SAT in the black/red box (Fig.7).

The three time series and corresponding histograms indicating the detection of an abrupt cooling event for each member are depicted in Figure 8. SST and SAT evolve

similarly and we find the mentioned high correlation between SST and SAT (correlation coefficient > 0.99 for ensemble means, upper and middle panel Fig.8) even for areas that are not exactly similar in their extent and location (masked deep convection area and black box Fig.7). Both ensemble mean years of detection are approximately in 2045 with a difference of less than 0.1 years. We conclude that using SAT instead of SST is a valid choice and does not change the main findings. The slight deviations could be a result of the black box not fully covering all masked deep convection sites. Therefore, the similarity in detection skill is likely to be even higher.
The SAT time series of the red box, in line with the reference region in Swingedouw et al. (2021) (Fig.7), is shown in the bottom panel of Figure 8. The SAT ensemble mean of this larger box shows almost no cooling and abrupt changes are not visible in the ensemble mean. Applying the same identification method results in the detection of 27 abrupt cooling events. From the analysis of the SPG SAT and SST (upper two panels), we know that abrupt cooling events do occur in almost all ensemble members. We conclude that the results are sensitive to the choice of the reference region. Using a mask that is too large and covers regions where no deep convection occurs leads to missing the detection of abrupt cooling events. For CESM2-LENS, more than two thirds of abrupt cooling events cannot be identified using the reference region suggested by Swingedouw et al. (2021).
In the second study on abrupt cooling in CMIP6 models (Swingedouw et al. (2021), first study by Sgubin et al. (2017) on CMIP5 models), one of the main conclusions was that CMIP6 models show a decreased risk of abrupt cooling in the subpolar NA. This is not necessarily true as we proved above. Additionally, we detect abrupt cooling events in CESM2 CMIP6 runs for three model runs forced by SSP585 applying our mask (Fig. 20). This scenario was discussed to show no abrupt cooling in any of the CMIP6 models. Hence, the question of whether the risk of abrupt cooling in the CMIP6 model ensemble actually decreases, or whether the change in the reference region causes a less skillful detection emerges.

Spreading of Collapsed Convection

To understand how the signal of collapsing deep convection propagates in the subpolar NA and where it appears first, we mask the northern NA for the area that exceeds 300 m in the annual maximum MLD (Fig.9). This threshold is smaller compared to the one used to mask the SPG deep convection sites and will result in a larger mask enabling us to analyze all regions of moderate deep convection. Note that this analysis is only done for the period from 2016-2100. The used threshold of 100 m is likely to be triggered early due to internal variability in regions that exceed the masking threshold only by a small margin.
We find the regions collapsing first to be the southern and north-western LS and parts of the Bay of Biscay off the coast of Spain and France. Besides these areas where the

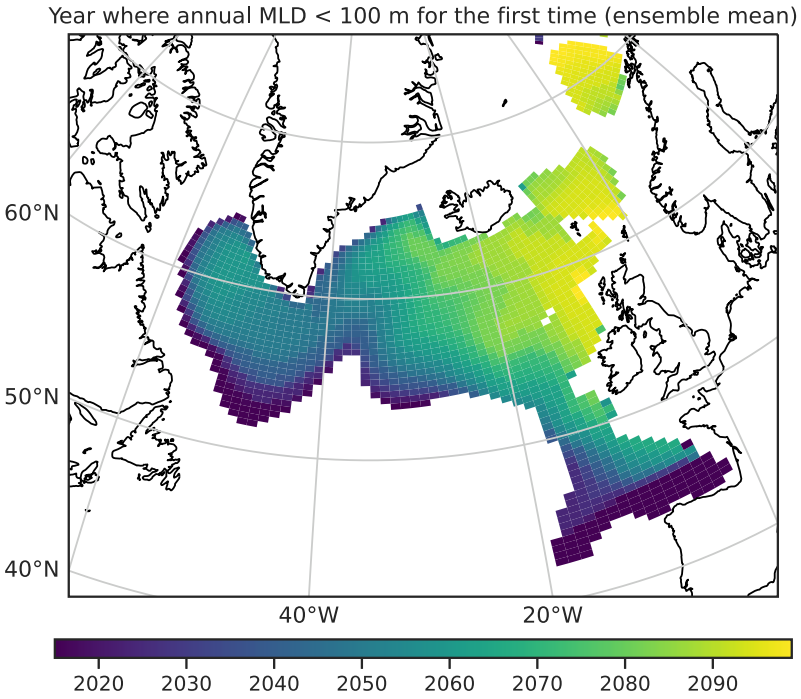

Figure 9: Subpolar NA, masked where the annual maximum MLD exceeds 300m in the historical data (1850-1950), showing the years when the annual mean MLD is shallower than 100m for the first time (ensemble mean).

threshold is probably too sensitive, we observe a clear pattern and find that the LS collapses the earliest, with the MLD falling below 100 m in the annual mean first at the southern borders of the LS and last in the center of the LS where the strongest deep convection site is located (Fig.2 & 9). Further, we identify the overall deep convection collapse propagating from west to east, with the Irminger Sea collapsing after the LS and the region south of Iceland collapsing last (when considering main deep convection sites Fig.2). At an even later point in time we observe a continuous decline and collapse of deep convection in the regions off the coast of the British Isles and an area off the coast of Norway in the central-eastern part of the Nordic Seas.

The collapse of deep convection in the LS is part of a larger-scale phenomenon, involving the entire subpolar NA region. Considering the size and strength of the LS deep convection site and its role in deep water formation through deep convection in the subpolar NA, the influence of named changes is likely to have the strongest impacts in this region. But overall, (moderate) deep convection is suppressed first in the western subpolar NA with the eastern subpolar NA following in the subsequent decades (see also Fig.4).

Drivers of Convection Collapse

As described in the introduction, a strong decline of sea surface density can lead to a collapse of deep convection, which in turn results in a shallow layer at the surface acting as a "lid" and preventing the deeper SPG water masses to lose heat to the atmosphere. Due to the shallower surface layer losing more heat in relation to its volume, a cold SST anomaly develops. Cold water is denser than warm water which already shows that it is unlikely for the SST to be the reason for the negative surface density anomaly that causes the convection collapse. With the main drivers of ocean density being temperature and salinity, we now investigate the development of SPG sea surface salinity (SSS).

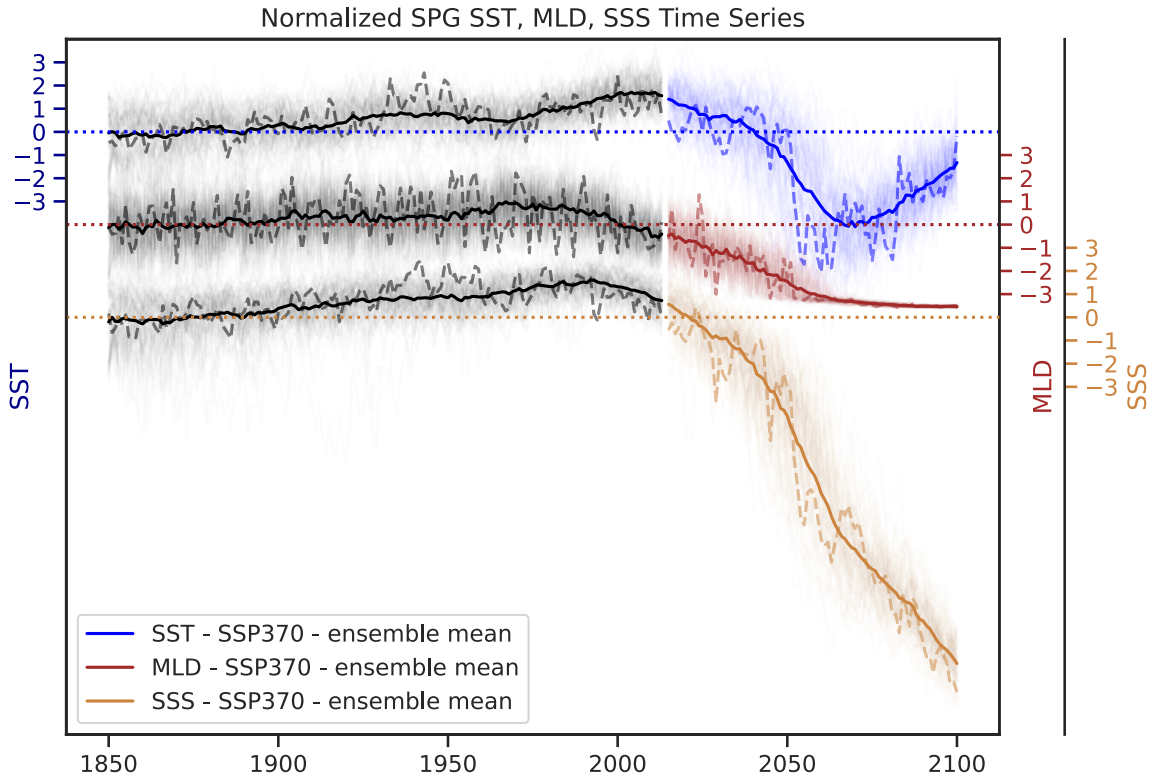

Figure 10: SPG SST (blue), MLD (red), and SSS (yellow) time series, normalized using mean and standard deviation calculated from 1850-1900 historical ensemble data. Dotted horizontal lines correspond to 1850-1900 mean, dashed lines correspond to the ensemble member '1001.001'.

Similar to before, we show the SST and MLD, but this time include the SSS of the SPG. We scale each time series with the corresponding means and standard deviations obtained from the historical data over the period of 1850-1900. This helps to compare

the magnitude of the changes for the different quantities.
Looking at the results in Figure 10 we can infer that SSS increases steadily from the beginning of the historical time series until 1990 when it peaks. Thereafter, SSS starts to decline and reaches it's corresponding historical (1850-1900) mean approximately in 2020. When the ensemble begins to show the abrupt cooling events, the rate at which SSS declines increases rapidly and only gets slightly smaller when SPG deep convection completely collapsed. This corresponds to a continuous freshening of SPG surface conditions even after the abrupt changes already happened and the new stable state is reached. SST and SSS both show a decline prior to the tipping events with the decline in SSS being stronger. The influence of SST on the surface density is opposite in sign and a decline in SST contributes to an increase in density. Hence, we can conclude that the salinity changes cause the negative density anomaly. Additionally, it is worth noting that the decline visible in all described quantities starts first in the MLD, then in the SPG SSS and the latest in the SPG SST.

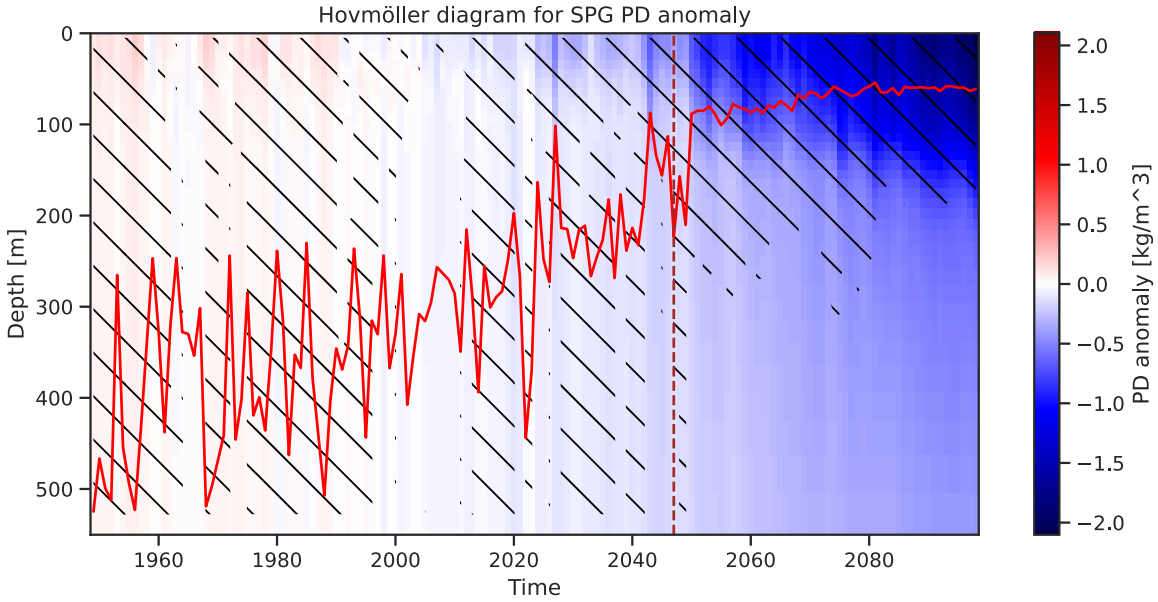

Figure 11: Hovmöller diagram for the SPG potential density (PD) anomaly (annual average) over the time and depth dimension for the single member '1001.001' of CESM2-LENS. Red solid line is the annual MLD and dashed vertical line indicates the year where tipping was detected. The hatched area indicates where the contribution of the salinity anomaly to the PD anomaly is positive and at least 10 times greater than the contribution of the temperature anomaly.

Adding to the information we obtain from analyzing the surface conditions, we investigate the salinity and temperature contribution to potential density (PD) anomalies in the

SPG from the surface to 550 m of depth. Below 550 m we find the PD anomalies to be similar in sign, but weaker. We therefore show only the results for the region above 550 m of the SPG water column in Figure 11. In theory, a convection collapse can also be triggered by the water masses below the surface showing a strong enough positive PD anomaly that hinders the surface water from sinking. This is not the case for the SPG convection collapse as we can infer from the Hovmöller diagram (Fig.11) where the whole water column shows a negative PD anomaly from the year 2000 onward. The negative PD anomaly is stronger closer to the surface and increases in magnitude towards the end of the century. We find a rather abrupt change in the magnitude of the PD anomaly shortly after the detected abrupt cooling (vertical dashed line) close to the surface. This jump in the PD anomaly is co-occurring with the last drop in the MLD. Additionally, we find that especially the PD anomaly close to the surface is dominated by changes in the SSS (hatched area of Fig.11). This again argues for the freshening of SPG surface conditions to be the main driver of the convection collapse with a MLD decreasing below 100m and the corresponding abrupt cooling. What cannot be explained yet is the initial decline in the MLD starting prior to the decline in SSS.

Dynamic Changes in the Subpolar NA

As mentioned in the introduction, a weakening or collapse of SPG deep convection results in an overall warming when considering the whole water column due to the decreased heat loss from the ocean to the atmosphere. This leads to a relaxation of the SSH gradient from the SPG center to the SPG border and therefore also a decline in the geostrophic flow (analogous to a weakening low-pressure system in the atmosphere). To analyze such dynamic changes in the subpolar NA we show the mean state of the SPG circulation in the historical data and how it changes towards the end of the century. The results are illustrated in Figure 12, where we clearly see that not only the overall strength of the circulation is changing, but also the shape and size of the SPG. Looking at the bottom panel of Figure 12, we find the strongest decline in the circulation to be located in the LS. Here, the BSF shows a decrease from approximately 50 to 25 sverdrup. Additionally, we identify regions of strong circulation decline in the Irminger Sea and south of Iceland, matching the regions where prior to the convection collapse the deepest MLD was located. Considering changes in the gyre size and shape, we observe a smaller gyre with the NA current shifted polewards. The north-eastern gyre extension into the Irminger Sea and the north-western extension into the LS become less prominent and a strong retreat of the south-eastern circulation limb is visible.

Figure 12 illustrates how the SPG circulation changed towards the end of the 21st century. With the discussed abrupt changes in the SPG SST, the question of whether

the circulation changes gradually or in a similar abrupt manner remains. We use the SPG strength index (see Section 3) to investigate the evolution of the gyre and the transition from the stronger circulation state, found in the historical data, towards the weaker circulation identified towards the end of the model simulation. Additionally, due to the close relation between SPG and AMOC (Section 2), we compute the AMOC strength time series. Although both, AMOC and SPG strength, are given in the same unit (Sverdrup), it is important to mention that the AMOC is the zonally averaged circulation in the vertical and meridional dimensions, and the SPG strength is a horizontal circulation averaged in the vertical dimension (see Section 3). Therefore, we do not compare the total values of the two circulations but their normalized time series or relative changes.
Figure 13 reveals that AMOC and SPG strength show a similar evolution in the historical time series from 1850 to 2000. Both time series display a constant mean strength in

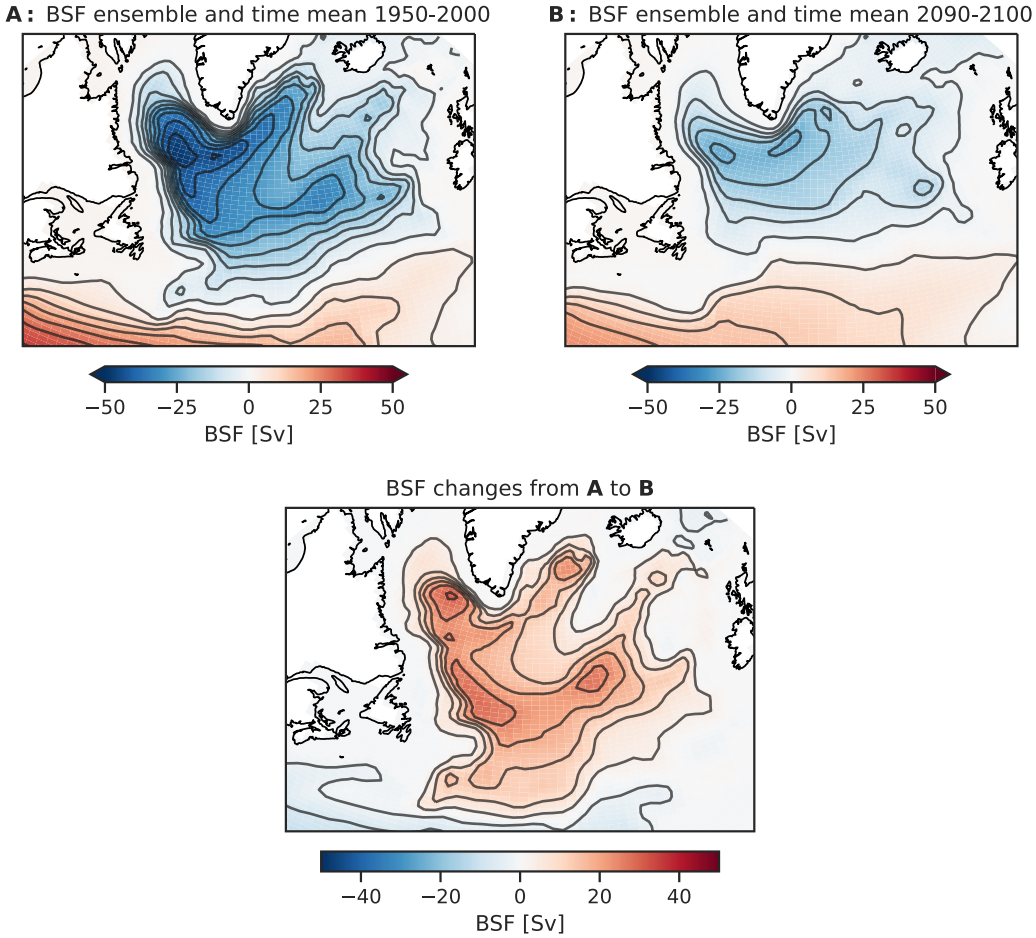

Figure 12: BSF for historical mean of the period from 1950-2000 (upper left), end of century mean for 2090-2100 (upper right), and the changes in BSF between the two (lower panel). Contour spacing corresponds to 5 [Sv].

the ensemble mean with two relatively sudden positive changes, one approximately in 1910 and one approximately in 1970, resulting in increased circulation strength. After reaching their maxima in the 1980s, we find the AMOC strength to gradually decline at a constant rate until the end of the 21st century and the SPG strength to show a strong and abrupt change in the year 2000. After this initial abrupt change, the rate of SPG strength decrease weakens constantly and the circulation seems to reach a new equilibrium towards the end of the simulation. In this new state, SPG strength declined by roughly 50 % and the variance decreased significantly (see Appendix Fig.27). The AMOC on the other hand does not show any signs of reaching a new equilibrium.
In the historical data, AMOC and SPG are mirroring each other closely. This close mirroring disappears at the beginning of the 21st century and the evolution of AMOC and SPG strength differ strongly. Due to the abrupt cooling and the collapse of convection, one could expect to observe a detectable signal in AMOC or SPG strength. Looking at Figure 13, this is not the case. Revisiting Figure 3 reminds us that the abruptness is only apparent in the SPG SST. The MLD declines gradually and no prominent abrupt changes can be observed, explaining in turn why the SPG circulation and the AMOC do not inherent similar signals during the corresponding abrupt cooling period (see also Section 2 for the link between MLD and SPG/AMOC).
With the described connection between AMOC and deep water formation in the SPG, it is not surprising to find both circulations to co-vary and show an overall similar evolution in the historical period. What is interesting on the other hand is the diverging evolution

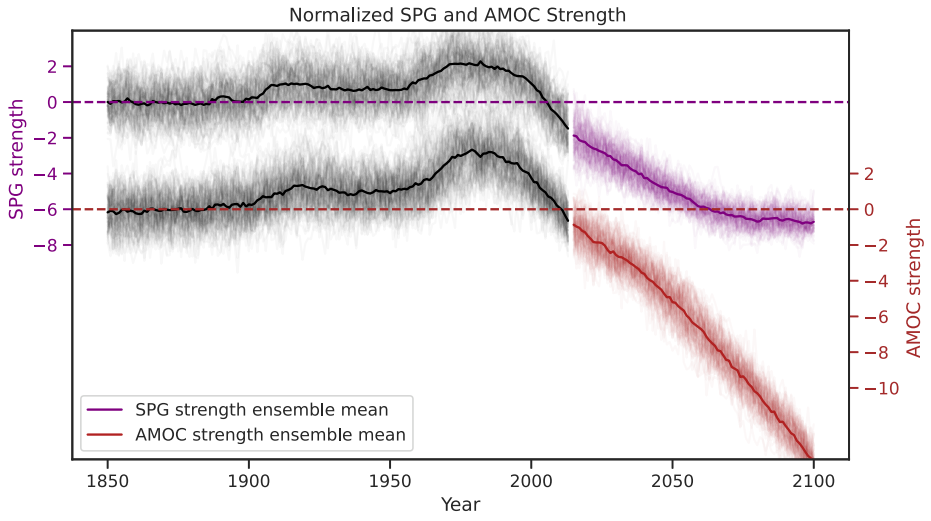

Figure 13: Ensemble AMOC (red) and SPG strength (violet) normalized with the corresponding ensemble data from 1850-1900. Black corresponds to the historical data from 1850-2015, colored time series corresponds to CESM2-LENS forced by SSP370. Thin lines are single ensemble members, thick lines are the ensemble means.

in the projection towards the end of the century. The new stable and unprecedented state of the SPG does not influence the ongoing decline of the AMOC. In turn, the continuous decline of the AMOC is not resulting in changes in the SPG strength towards the end of the 21st century. Keeping the close mirroring of both in the historical period in mind, this points to a change in the interplay between SPG and AMOC. One possible explanation is that the new weak SPG state is not sensitive to changes in the AMOC and the other way around.

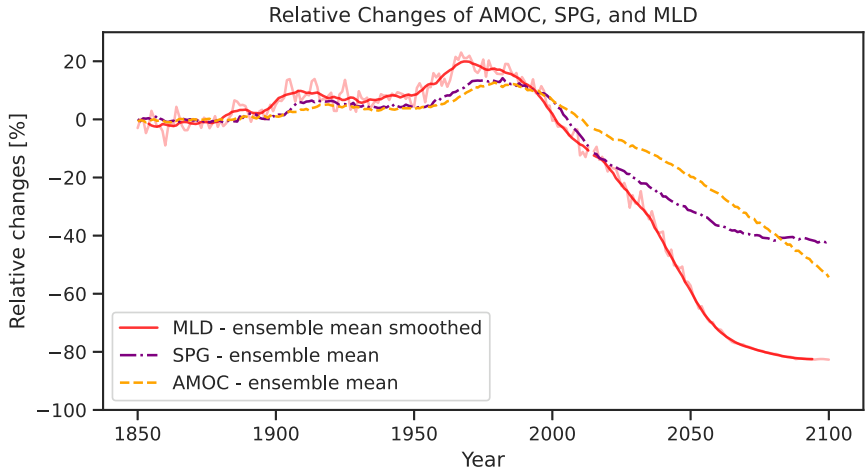

Figure 14: Relative changes in [%] of AMOC (orange and dashed), SPG strength (purple and dash-dotted), and MLD (red and solid lines)(with respect to 1850-1900 historical mean). Smoothed MLD ensemble mean time series is computed using a 10 year moving average function.

The comparison of the relative changes of the ensemble means in Figure 14 suggests that changes in the MLD lead to changes in AMOC and SPG strength. The two above-mentioned abrupt increases of SPG and AMOC strength in the historical period are both apparent in the MLD approximately 10 years earlier. The described close mirroring of AMOC and SPG is even more apparent comparing their relative changes. We find that AMOC lags changes in the SPG by multiple years, but closely follows the SPGs evolution. As mentioned in the introduction (Section 2), a lot of work points to this relationship with the LS (largest region of the SPG mask; Fig.2b) proving to have a high skill in predicting AMOC variability.
With LS deep convection disappearing, observing a decline in AMOC variability and SPG strength variability is not surprising. Without deep convection, the link between wind-driven heat loss, density perturbations, and the gyre circulation cannot be maintained. Therefore, one important source of SPG strength and AMOC variability vanishes (Fig.13 and Appendix Fig.27).

The strong decline that eventually results in the subpolar NA reaching the above described new state without deep convection is again first apparent in the MLD. The onset of the strong decline in AMOC and SPG strength happens simultaneously and we find the already described evolution, with the strong similarities of AMOC and SPG strength disappearing towards the end of the model simulation.

Sub Ensembles

Another advantage of CESM2-LENS consisting of 100 members is the possibility to determine sub ensembles. This allows for a straightforward investigation of the impacts of a SPG deep convection collapse and the corresponding abrupt cooling of SPG SST. With internal and external components determining the evolution of SPG SST, we observe different years of abrupt cooling in Figure 4. Natural variability of the drivers of deep convection collapse events leads to some members showing an earlier onset of abrupt changes than others.

Selection of Sub Ensemble Members

The idea is to determine two sub ensembles consisting of 10 members each, with one sub ensemble representing early convection collapse and the other representing late convection collapse. Assessing differences between these two sub ensembles in their evolution of the already discussed quantities will help to identify the main drivers contributing to an early or late onset of convection collapse. Additionally, comparing climatologies of the two, with one of them already gone through the abrupt cooling and the other one not, will enable us to investigate the effect abrupt cooling has on large-scale atmospheric conditions (Section 6). The novelty of this approach is that we can assess the effect of abrupt cooling excluding the effects of global warming. With both sub ensembles experiencing the same additional radiative forcing, attributing differences between the sub ensembles to the abrupt cooling is likely to be more accurate.
To determine these two sub ensembles, we compute the ensemble variance for each time step. With abrupt changes in SSTs forced by a convection collapse being much bigger in magnitude compared to the internal variability of the system prior to the abrupt cooling events, the ensemble variance is expected to increase when the first ensemble members begin to show abrupt cooling and decrease again when the majority of ensemble members reached their new stable state. We observe this behavior in Figure 3 and validate these assumptions by plotting described ensemble variance and additionally the SPG SST. We find a strong increase in the ensemble variance in proximity of the abrupt cooling events

between 2045 and 2058 (Fig.15).

For clarification, the described increase in variance is not the often proposed increase in variance a tipping element shows when approaching its critical threshold (Lenton, 2011). Instead, it is caused by the magnitude of the abrupt changes overshadowing the natural ensemble spread prior to the abrupt changes and the abrupt cooling events occurring in different years for each ensemble member.
To subdivide into the two sub ensembles, we pick the 10 members that show the coldest and the 10 members that show the warmest SST at the time of maximum ensemble variance (vertical line Fig.15). The 10 warmest and coldest members now represent the early collapse sub ensemble (ECE) and late collapse sub ensembles (LCE).

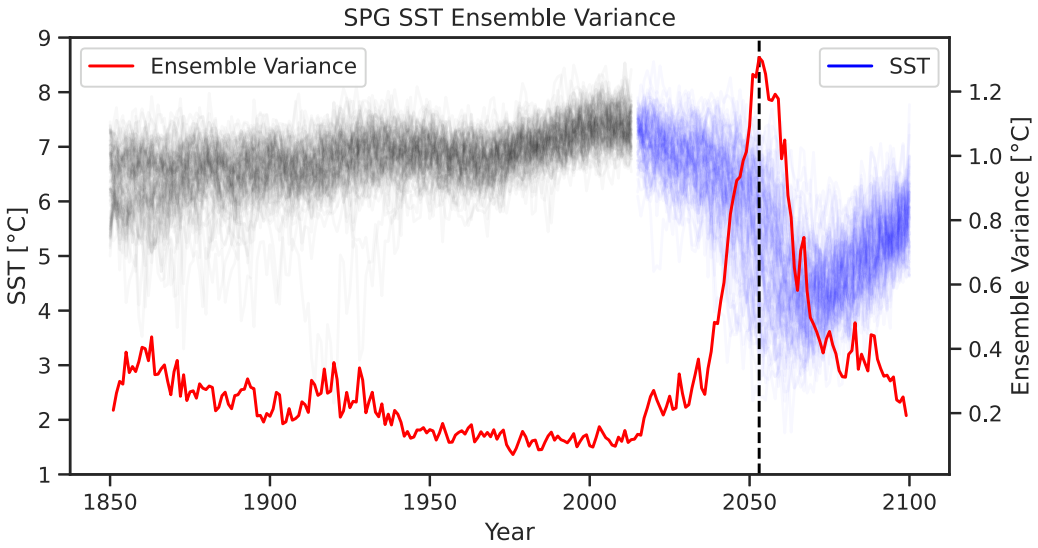

Figure 15: SPG SST time series of all ensemble members as in figure 3. Red line shows the SPG SST ensemble variance for each year. Dashed vertical line indicates the year of maximum ensemble variance (year 2053).

The result of this subdivision is shown in Figure 16 for the SST time series and we find a clear difference in the evolution of the two sub ensembles. Shortly after 2020, the ECE shows a decreasing mean SST while the LCE shows almost no changes in SPG SST. The ECE shows the described abrupt cooling beginning in 2030 and lasting until 2053. Here, we find the ECE and LCE to show the biggest difference. The ECE has reached its lowest SPG SST and is almost 4°C colder than the LCE that has not started its rapid decline. After 2053 the LCE enters its abrupt cooling phase and the ECE already begins to show the overall increasing SPG SST as described in section 4. After 2070, when the LCE has gone through the rapid transition, the

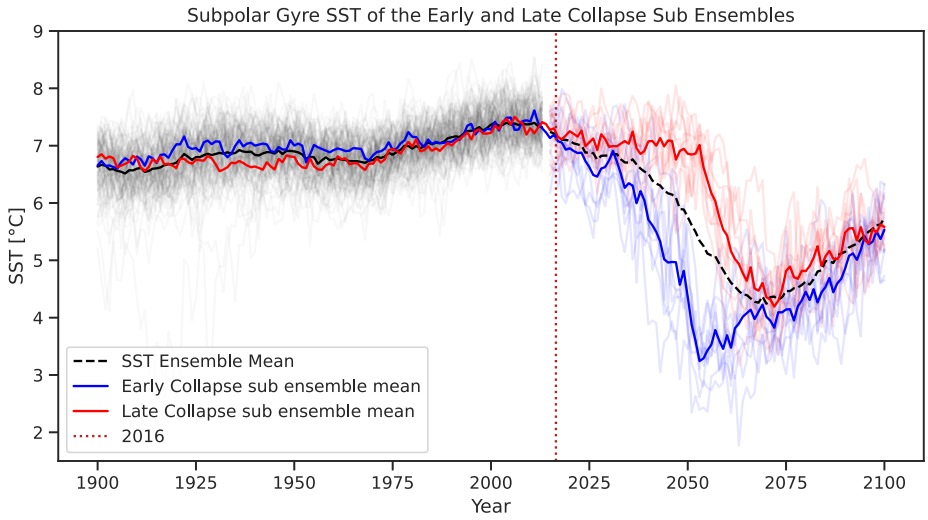

Figure 16: Shown are the two sub ensembles. Thin lines are the single members, thick lines are the (sub) ensembles means. Red/Blue depicts the 10 members that show the warmest/coldest SPG SST at the point of maximum ensemble variance. Red is referred to as late collapse ensemble (LCE), blue is referred to as early collapse ensemble (ECE). Vertical dashed line indicates the first year where the two sub ensemble time series are significantly different for the first time and stay significantly different until the abrupt cooling events (see supplementary method 9).

SST of both sub ensembles are only slightly but constantly shifted and follow a similar positive trend. In the last 10 years of the century, no differences between the two sub ensembles can be identified and ECE and LCE means are similar to the large ensemble mean.

Sub Ensemble Time Series

The division results in two ensemble member groups that can be seen as a lagged composite, with the LCE abrupt cooling lagging the ECE abrupt cooling. By investigating how the time series of other quantities of the two ensembles evolve prior to the abrupt cooling events, we can identify early signs of divergence. This allows for a more accurate analysis of drivers of SPG convection collapse. Quantities that do not contribute to the development of the anomalous surface conditions are unlikely to show an ongoing difference between the ECE and LCE in the years preceding the convection collapse. Finding a prolonged significant difference between ECE and LCE will therefore emphasize the role of the corresponding quantity in the development of the abrupt cooling and convection collapse. When assessing the results, it is crucial to consider that a driver of abrupt cooling caused by deep convection can affect other quantities in the subpolar NA

and the atmosphere that do not influence deep convection. These quantities could show a similar difference between the sub ensembles despite not contributing significantly to the development of the abrupt cooling events.

In Figure 17 we find that for all already discussed variables the sub ensembles are significantly different in the years leading to the collapse of deep convection. The MLD sub ensembles are significantly different from 2009 onward. Due to the strong natural variability in the MLD, the sub ensemble means do overlap after 2009, but the used window size for testing the significance of the difference is large enough to prove the overall difference in the years from 2009 until the collapse of convection (see additional method 9). The diverging ECE and LCE time series of SSS are less noisy and we identify a decrease in SSS. The ECE SSS decreases at a stronger rate resulting in fresher surface conditions. As discussed earlier, this freshening is the main reason for the complete and final collapse of convection. Noteworthy is the early onset of a constantly fresher SPG in the ECE already starting in 2010.
Furthermore, AMOC and SPG strength prove to be different in the ECE and LCE as well. The SPG strength sub ensembles are different from 2008 onward and the AMOC strength sub ensembles from 2009.
Striking is the earlier onset of the described detectable difference between ECE and LCE in all quantities compared to the SPG SST, although the SST is the variable used to define the two sub ensembles in the first place. This again points to the SST playing no significant role in driving the collapse of deep convection. Additionally, we find the years when the first signs of diverging sub ensembles are detected to be similar and only slightly different for the MLD, SSS, SPG strength, and AMOC strength. This is not surprising with many studies linking these quantities and explaining how they co-vary (see Section 2).

Towards the end of the model simulation, the SPG strength sub ensembles behave similarly again and are not significantly different from each other or the large ensemble mean. This coincides with the time when the SPG strength reached a new stable state and does not show an ongoing trend. The evolution of the AMOC is different and the observed difference between the ECE and LCE AMOC strength stays significant until the end of the century. In other words, this observation suggests that towards the end of the model simulation, SPG strength variability is driven by internal variability, and internal variability eliminated any preceding differences between the two sub ensembles. The AMOC on the other hand stays different between the ECE and LCE. This implies that internal variability is not strong enough to eradicate the lagging evolution of AMOC strength, suggesting a forced response strong enough to not be overshadowed by internal variability. One explanation could be a positive feedback loop leading to the AMOC decline. With the same feedback loop driving both sub ensemble AMOC evolutions, the year in which the positive feedback loop starts to control AMOC matters for the ongoing development. This in turn would point to the AMOC reaching a tipping point at the same time as the SPG starting its transition towards a weaker stable state.

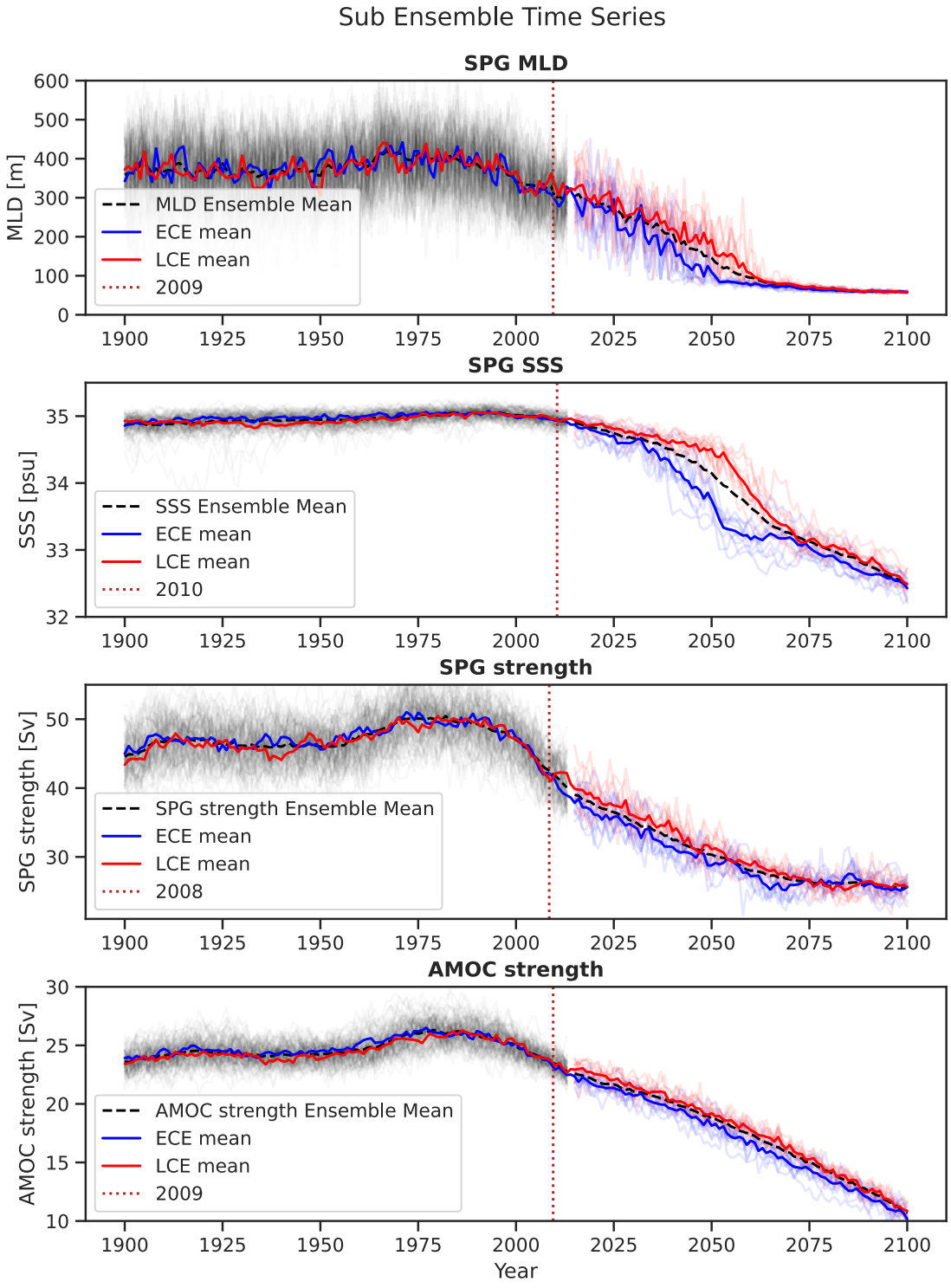

Figure 17: ECE and LCE time series for SPG MLD, SPG SSS, SPG strength, and AMOC strength. Similar to Fig.16, vertical dashed lines indicate the first year where the two sub ensemble time series are significantly different for the first time and stay significantly different until the abrupt cooling events (see supplementary method 9).

Forcing Scenario Dependence

We will now take a look at the effect different forcing scenarios have on the evolution of deep convection in the SPG. For this analysis, we use additional CESM2 model runs that were computed as a contribution to CMIP6. Identifying how SPG surface conditions vary when the external drivers in the form of greenhouse gas emissions and aerosol forcing are altered will further help to understand potential causes of a collapse of deep convection and if a stronger forcing results in an earlier collapse of SPG deep convection.

CESM2-LENS vs. CESM2 CMIP6

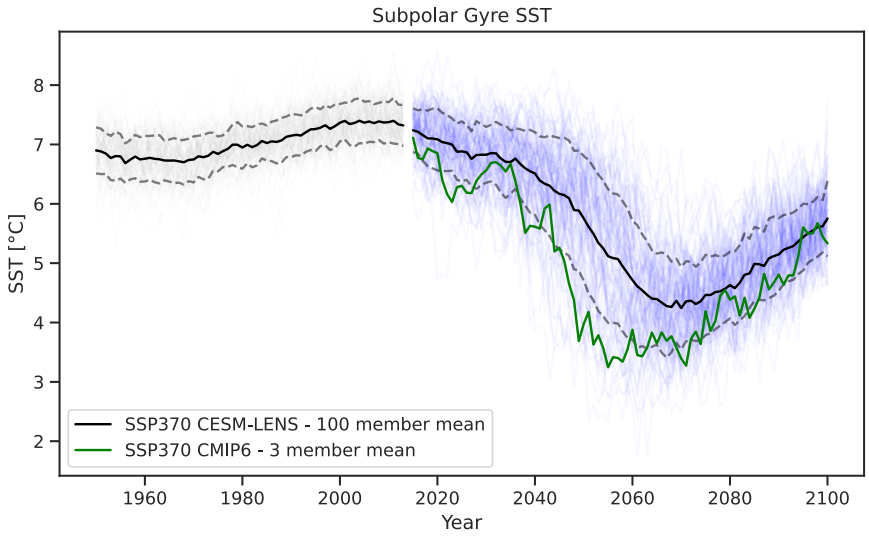

Figure 18: SPG SST including the mean of three CESM2 CMIP6 model realizations forced with the same forcing scenario as CESM2-LENS (SSP370). Solid lines are the corresponding ensemble means, dashed lines indicate $+/-$ one standard deviation of the large ensemble time series.

Before comparing all forcing scenarios we take into account, we examine the three CESM2 CMIP6 model runs forced by SSP370 in relation to CESM2-LENS also forced by SSP370. Figure 18 shows the SPG SST for CESM2-LENS and the mean of the three CESM2 CMIP6 members. The CMIP6 runs deviate strongly from the large ensemble mean. In many years, especially in the years where the abrupt SST change is identified, this deviation exceeds one standard deviation. The results from Section 4 suggest that changes in the driving variables already in the historical period are likely to influence the time of the onset of convection collapse events. The CMIP6 runs have different historical simulations compared to CESM2-LENS. Due to this potentially large dependence on the historical simulation, we will compare only the CESM2 CMIP6 runs.

These runs share the same historical simulation preceding the onset of the different forcing scenarios in 2015. The internal variability of the onset of abrupt cooling and the end of the convection collapse (see Fig.20) on the other hand are used to assess whether any detected difference between the forcing scenarios is attributable to changes in the forcing.

Scenario (In)dependence

The results of SPG surface conditions and MLD dependence on changes in the external forcing in the form of different SSP scenarios are shown in Figure 19. The timing of abrupt cooling, complete collapse of convection, and decline in surface salinity do not reveal signs of dependence on the SSP forcing scenario. The SST drop is decreased in magnitude in the stronger forcing scenarios. After the abrupt cooling, we observe a strong dependence of the ongoing SST evolution on the forcing scenario. SST in the SSP126 scenario does not increase after the abrupt cooling. The drop of SST in SSP370 is similar to SSP126, but after the abrupt changes (from $\approx$ 2060 onward) SST shows a positive trend. SST in SSP585 exhibits the abrupt changes at a similar time but does not decrease as much as in the other two scenarios. The following strong positive SST trend is larger than for the weaker SSP370 forcing scenario.
The evolution of the MLD exhibits even greater resemblance, with the forcing scenarios that are the most different (SSP126 - blue and SSP585 - red) showcasing a similar development and decline. For the SSS the picture is not different and the visible differences are likely driven by internal variability.

Figure 20 depicts the already discussed spread in the detection of abrupt cooling events and the final collapse of deep convection (light blue and light red histograms). The dashed vertical lines are plus and minus one standard deviation of the corresponding mean. They represent the spread in the years of the occurrence of collapse events that is attributable to internal variability. Additionally, Figure 20 shows the years of detection for the three SSP scenarios. The first striking observation is the shift towards an earlier beginning and end of the described abrupt cooling events. With the already mentioned strong dependence on the historical simulations determining the onset of abrupt cooling to a large extent (see section 4), it is likely that the shift towards earlier detection in all SSP scenarios is resulting from differences in the historical CESM2 CMIP6 runs.
Nevertheless, we can infer that the timing of abrupt cooling in the subpolar NA is not influenced by the forcing scenario, but rather by natural variability. This becomes evident from the strong variation in detection years for the same forcing scenarios, which exceeds the differences between the scenarios. Considering the independence on the forcing scenario and the overall earlier abrupt cooling in all CMIP6 runs compared to the CESM2-LENS simulations, the only possible explanation lies in large-scale changes in the

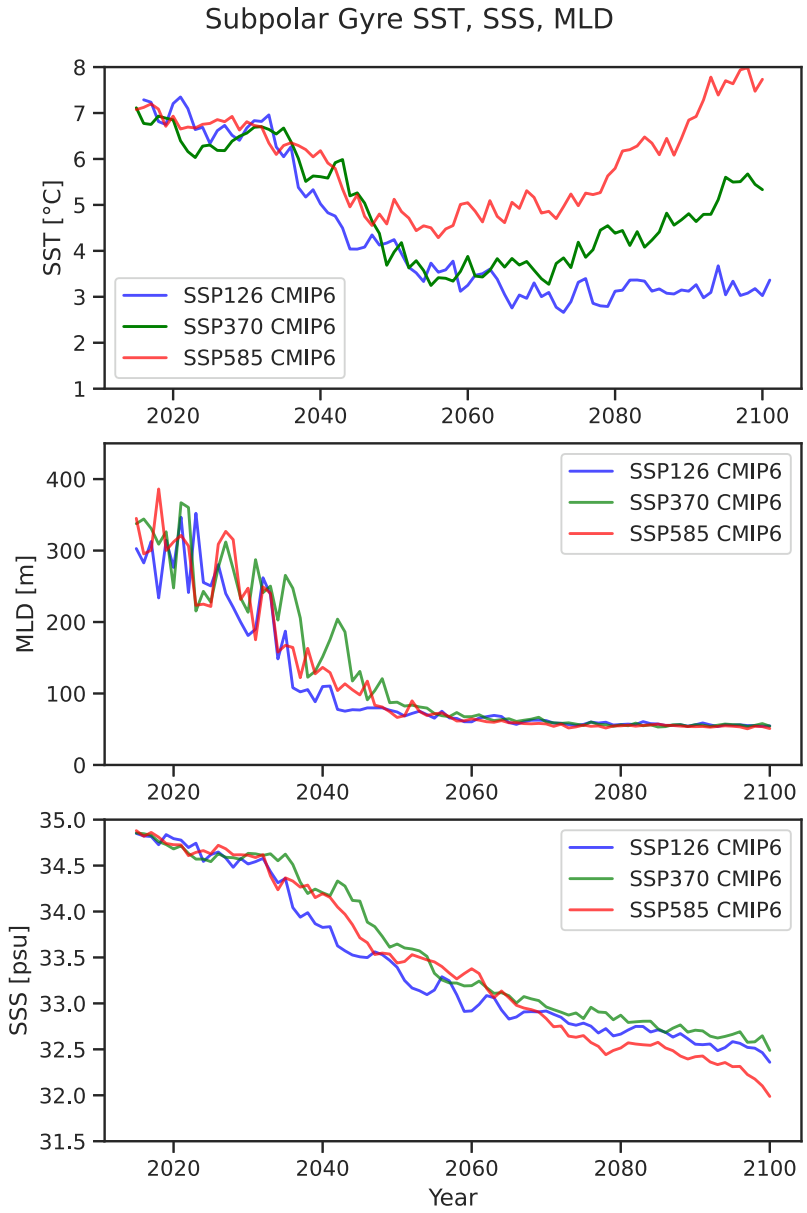

Figure 19: SPG SST (upper panel), MLD (middle panel), and SSS (lower panel) for three different SSP forcing scenarios. Shown is the mean of the three available CESM2 (CMIP6) model realizations for each SSP scenario. Red is SSP585, green is SSP370 (same forcing as in CESM2-LENS), and blue is SSP126.

historical runs making a collapse of deep convection decades later inevitable. Therefore, a tipping point leading to a convection collapse and abrupt cooling would be reached decades before the described prominent anomalies in the form of abrupt cooling become visible.

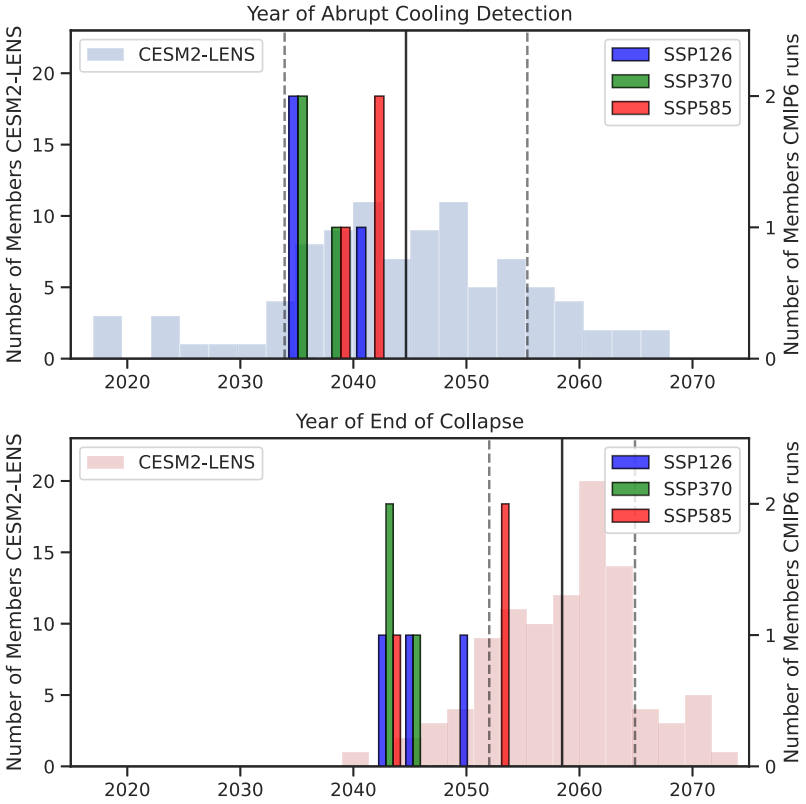

Figure 20: Histograms indicating the years of abrupt cooling detection (upper panel) and the years of final convection collapse (lower panel). Light blue and red histograms (background) as in figure 5, grey dashed vertical lines indicate plus and minus one standard deviation for the already discussed histograms, solid vertical lines indicate the corresponding mean, and bold colored are the histograms for the three model runs for each SSP forcing scenario. Note that the deviation of the SSP scenarios years of detection away from the large ensemble mean year of detection is likely due to the different historical model runs preceding the forced runs (as discussed in Section 18).

5 Where lies the tipping point?

The sub ensemble results and the forcing scenario independence both suggest the tipping point to not lie in the deep convection collapse itself. Observing no difference in the timing of the abrupt cooling events for forcing scenarios as different as SSP126 and SSP585 is pointing to the SPG being insensitive to external forcing in the years preceding the abrupt SST cooling. We therefore conclude that the anomalous changes in the quantities linked to convective activity have potentially reached a point where they enter a positive feedback loop. This positive feedback loop and the discussed ongoing decline in SPG MLD, SSS, and SST that already started decades prior to the abrupt cooling could explain why named variables evolve without reacting to changes in the external forcing. The results of these discussed closely related variables could be a hint pointing towards a tipping point in the whole SPG circulation.

The idea of a tipping point in the subpolar NA that does not lie in the deep convection itself, but in the whole SPG circulation is not new. As Andreas Born et al., 2014 show using a simple box model, the SPG can have two stable states. In the state of stronger gyre circulation, eddy advection of boundary current water masses that are higher in salinity towards the gyre center help to maintain deep convection and keep the water column density high. Consequently, also the SSH and density gradients are strong which keeps the general SPG circulation at a level that maintains this feedback loop. If now an initial decline in gyre strength weakens the eddy advection from the boundary current to the center, or the boundary current becomes fresher, the described feedback loop would weaken the convective activity at the gyre core, relax the SSH and density gradient and therefore result in an overall decline of the SPG circulation. As a consequence, the advection of more dense water masses towards the gyre center would further decline and a tipping point is surpassed, resulting in an ongoing decline towards a new and weaker stable state without deep convection at the SPG deep convection sites.

Considering our findings, this theory is plausible and could explain the overall large-scale changes in the subpolar NA. Assessing the MLD, SSS, and SPG strength decline in CESM2 fits the described narrative. The positive feedback loops and bistability of the SPG circulation as suggested by Andreas Born et al. (2014) could explain the evolution of SPG conditions we described above. This has two important implications. One is that the actual tipping point is the SPG circulation and is reached decades before the abrupt cooling occurs, and the other is that the often-mentioned collapse of deep convection leading to abrupt surface cooling is only one of the last steps toward the new stable state of the SPG. In other words, the tipping point causing the abrupt surface cooling and collapse of deep convection also mentioned in Armstrong McKay et al. (2022) is reached decades before the event and the estimated thresholds would not indicate the

tipping point, but only the most prominent but lagged signal of a larger scale tipping event.

Is a Transition to a weak SPG Circulation Inevitable?

Assuming CESM2 is doing a good job at mimicking our real-world climate system, our results lead to the conclusion that the SPG circulation is already on its way to the new stable state, significantly weaker in strength and without deep convection in its center. Therefore, the question of whether we have already passed the tipping point decades ago, or CESM2 is falsely projecting described transition is justified.
A stable SPG circulation is mainly driven by changes in the atmospheric forcing and increased or decreased heat loss at the deep convection sites. Due to SSS being stable and not changing significantly, the density and convective activity is controlled by temperature changes. In turn, when the SPG circulation approaches its tipping point, the SSS decreases and is likely to become the main driver of SPG variability. A recent study using re-analysis data suggests that the SPG was predominantly driven by temperature changes until 2000. Afterward, a change toward an increased SSS impact on SPG variability is identified (Biri et al., 2019). Is this evidence for passing the tipping point of the SPG?
Since summer 2014 the Overturning in the Subpolar North Atlantic Program (OSNAP) is operating and measuring the overturning circulation with arrays located in the LS and between Greenland and the British Isles. The first 21-month OSNAP record is assessed in the study of Lozier et al. (2019). Here, the often-suggested strong link between LS deep convection and AMOC variability could not be identified. Although the 21-month OSNAP record is short, these findings emphasize that coupled climate models still struggle with the realistic representation of the subpolar NA.
Additionally, Swingedouw et al. (2022) prove that modelling deep convection in the subpolar NA is sensitive to the model resolution. High-resolution mesoscale eddy permitting ocean models show an increased advection of boundary current water towards the SPG deep convection sites. This shows that parameterizing eddies, as in CESM2, might result in a less skillful projection.
One needs to further consider that the melting ice sheets of Greenland and the corresponding freshwater runoff are not implemented in CESM2. Freshwater reaching the deep convection sites and diluting saline surface waters will weaken deep convection, the gyre circulation, and potentially the AMOC (Swingedouw et al., 2022). On the other hand, the freshening of the boundary currents can lead to an increase in the gyre core to gyre periphery density gradient. This has a strengthening effect on the circulation and a strong freshwater pulse is identified to be a potential explanation for the last transition of the SPG from its weak to the current strong state 8200 years ago (A. Born et al., 2010).
The majority of our understanding of the coupled LS deep convection, SPG circulation,

and AMOC system is not based on climate records but rather originates from theory and simplified models. Small changes in climate model resolution already have a large impact on the results and climate models show a large spread when it comes to projecting the subpolar NA's evolution (see Section 2). Hence, answering the question of whether we are approaching, or have already passed the SPG tipping point in the real world is not possible yet.
Therefore, more work needs to be conducted on correctly modeling the SPG, including Greenland ice sheet meltwater runoff. With a growing OSNAP record, the robustness of comparing model results with records will grow and further help to assess the skill of climate models in simulating the subpolar NA.

Still, in the case of an abrupt cooling in the subpolar NA of similar magnitude, as observed in CESM2, it is important to understand the potential consequences for the state of the atmosphere. Hence, we assess these impacts on atmospheric conditions in the following section.

6 Impacts of abrupt cooling in the Subpolar NA on Atmospheric Conditions

Anomalous sea-surface conditions impact atmospheric conditions not only in the direct proximity of the SST anomaly. The influence of the Atlantic multidecadal variability (AMV) on the large-scale atmospheric circulation is well studied and the SPG region is playing a major role in determining the phase of the AMV (see Section 2). But with abrupt cooling events linked to the shutoff of deep convection producing cold SST anomalies with a magnitude that hasn't been observed in the last centuries, it is important to understand consequences of a subpolar NA without active deep convection.

Changes in the Surface Heat Flux

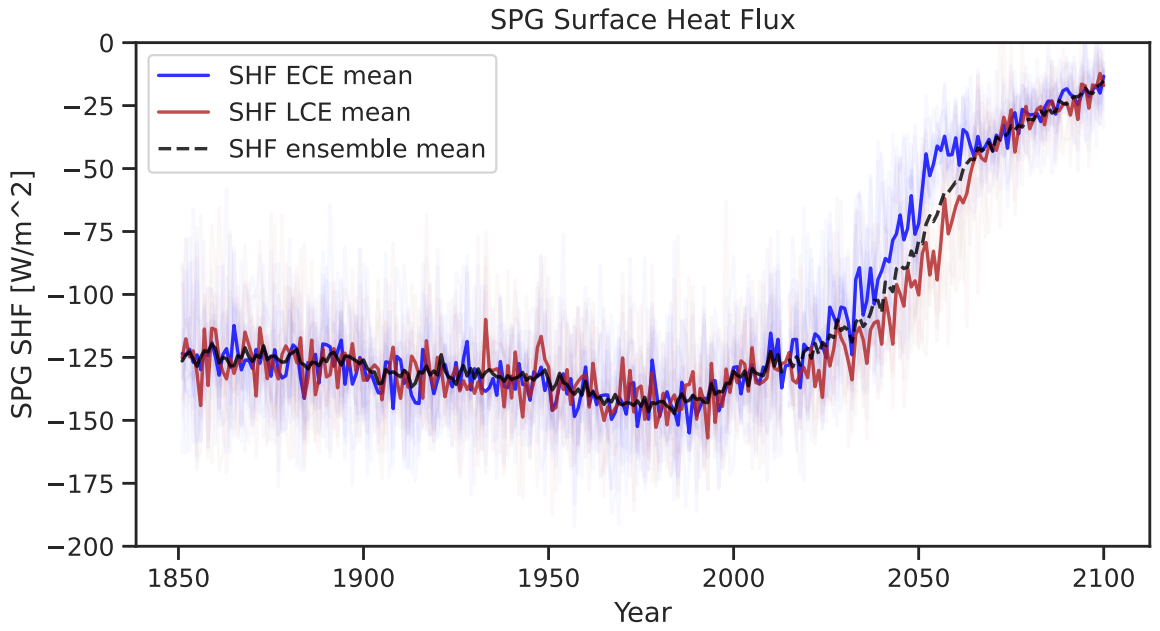

Figure 21: Annual SPG SHF development of the two sub ensembles, blue being the ECE and red being the LCE. Solid lines are the sub ensemble means, thin lines the single members. Black dashed line is the large ensemble mean. Negative SHF translates to the ocean loosing heat to the atmosphere.

The subpolar NA is losing heat to the atmosphere due to relatively warm ocean temperatures compared to colder atmospheric conditions. The SST cools due to this heat loss, increases in density, and is convected to greater depths. In exchange, warmer deep water masses reach the surface. When deep convection is weakened the transport of warm

water to the surface is reduced and the initial strong ocean-atmosphere temperature gradient is weakened. This is in line with what we find for the development of the SHF shown in Figure 21. First, the SHF decreases until reaching its minimum around 1980. Then, we observe an increase with a strong positive trend in the period where we identified the most abrupt changes in the SST and SSS. After 2060, SHF further increases with a slightly reduced positive trend. The overall decrease in SPG heat loss is large and in the period from 2000 to 2100, SPG SHF changes from $-150\frac{W}{m^2}$ to $-25\frac{W}{m^2}$ in the ensemble mean.

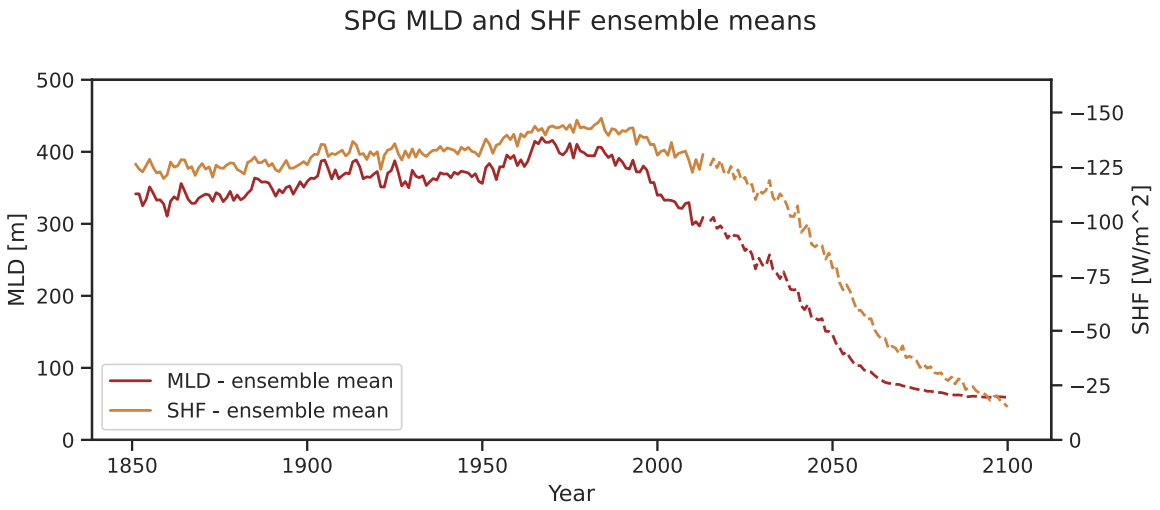

Figure 22: Ensemble mean SHF as in Figure 21 (black dashed line), but with reversed y-axis, and ensemble mean MLD. Solid lines show the historical period and dashed lines show the projection from 2015 to 2100.

The described relation between MLD and SHF is apparent in Figure 22. In the historical period, the similarities are striking and the corresponding correlation coefficient is > 0.9 (anticorrelation when the y-axis is not flipped). When the large-scale changes in the whole SPG begin ($\approx$ year 2000), the close relation is still apparent, but the SHF reaction to the strong decline in MLD appears lagged. Here, we find the largest correlation coefficient of ≈ -0.98 for a lag of approximately 10 years (Appendix Fig.28). This lagged response is likely caused by the gyre circulation and potentially the AMOC adjusting to the density changes in the gyre center due to increased or decreased SHF. This adjustment is slower and changes the whole state of the subpolar NA and therefore the corresponding signal in SHF emerges later. The immediate adjustment is visible in the strong similarity of the year-to-year fluctuations of SHF and MLD.
Comparing the ECE and LCE (Fig.21), we observe the expected drift in the years of abrupt cooling, where the SPG SST difference is the largest. The ECE shows an earlier decrease in the absolute SHF. After both sub ensembles collapsed ($\approx$ year 2070), no

difference can be observed and ECE and LCE means share an ongoing similar evolution around the large ensemble mean.

The Role of Atmospheric Forcing in the Development of Abrupt Cooling

Comparing two sub ensembles of CESM2-LENS at the same time step will unveil some of the potential impacts of an abrupt cooling in the subpolar NA. But with the atmosphere playing a potential driving role in the development of convection collapse events, it is not sufficient to analyze only the difference at one single time step. Driving patterns forcing the development and signals forced by the abrupt cooling can overlap and be hard to distinguish. We therefore show the difference between the ECE and LCE for SST, SAT, and PSL in the years preceding the convection collapse and the years following in Figure 23. Identifying constant signals approaching the years of maximum SST difference (2003 - 2043) and a change where SST and SHF differ the most from ECE to LCE (2053) will help to differentiate between driving patterns and consequences of abrupt cooling.
Starting in the year 2003, with the SST showing no difference yet, we cannot identify a strong or ongoing signal in the SAT and PSL. In 2013, with still no SST difference observable, we find a large scale positive PSL difference over Greenland and the subpolar NA, and a negative PSL difference over the subtropical NA and Europe, similar to a negative phase of the North Atlantic Oscillation (NAO) (Wanner et al., 2001). This pattern proves to be consistent and we identify it in the following years until 2043. The persistence and early emergence prior to the onset of the SST difference between the ECE and LCE highlights the role of the atmosphere in the development of abrupt cooling events. Nevertheless, it is important to note that the large-scale changes in ocean circulation and the decrease in SPG MLD and SSS start earlier and are the dominating drivers of convection collapse events (Fig.17). We therefore conclude that the atmosphere plays a minor role in reaching the tipping point of the whole system, but a major role in determining when exactly the collapse of deep convection and consequential abrupt cooling occurs.
In 2053, where the difference in SSTs is largest, the negative NAO-like signal vanishes and we observe a different pattern in the PSL difference. With the LCE now being close to the onset of the abrupt changes, one can expect the positive NAO-like pattern to vanish. This is to be expected if one of the underlying causes of the lagged convection collapse of the LCE is the described positive NAO phase of the preceding years. We conclude that the PSL difference at the time of maximum SST difference (2053) is likely to be a consequence of the cold SST anomaly.

We identify the first weak SST difference in 2023 after the onset of described negative

NAO-like signal. In the following years, the spatial extent and magnitude of the SST difference increase until 2053 when we observe the strongest difference. In the masked SPG region, the SST difference decreases in the following years, but in other regions we find a lagged peak of SST difference. This is in line with the overall spatial development of the convection collapse in the subpolar NA. In Figure 9 we observed the West to East developing MLD collapse, which is likely the reason for described development of SST difference and lagged response of the eastern subpolar NA.
SAT difference in the NH develops similarly to the SSTs. Investigating the difference between the ECE to the LCE, we find that the polar and subpolar regions show persistent colder SATs in the ECE. The magnitude of this difference is largest at the time we also observe the biggest difference in SSTs. The overall SAT difference weakens when SST difference weakens, with one exception. In the Arctic Ocean, the difference in SAT is consistent and shows no signs of weakening even for a vanishing SST difference. This could be a sign of the abrupt changes in the subpolar NA affecting the onset or continuous development of the state of the Arctic Ocean that appears lagged from that point onward. Another explanation could be the described continuous difference in the state of the AMOC influencing the state of the Arctic Ocean (see Fig.17 lower panel).

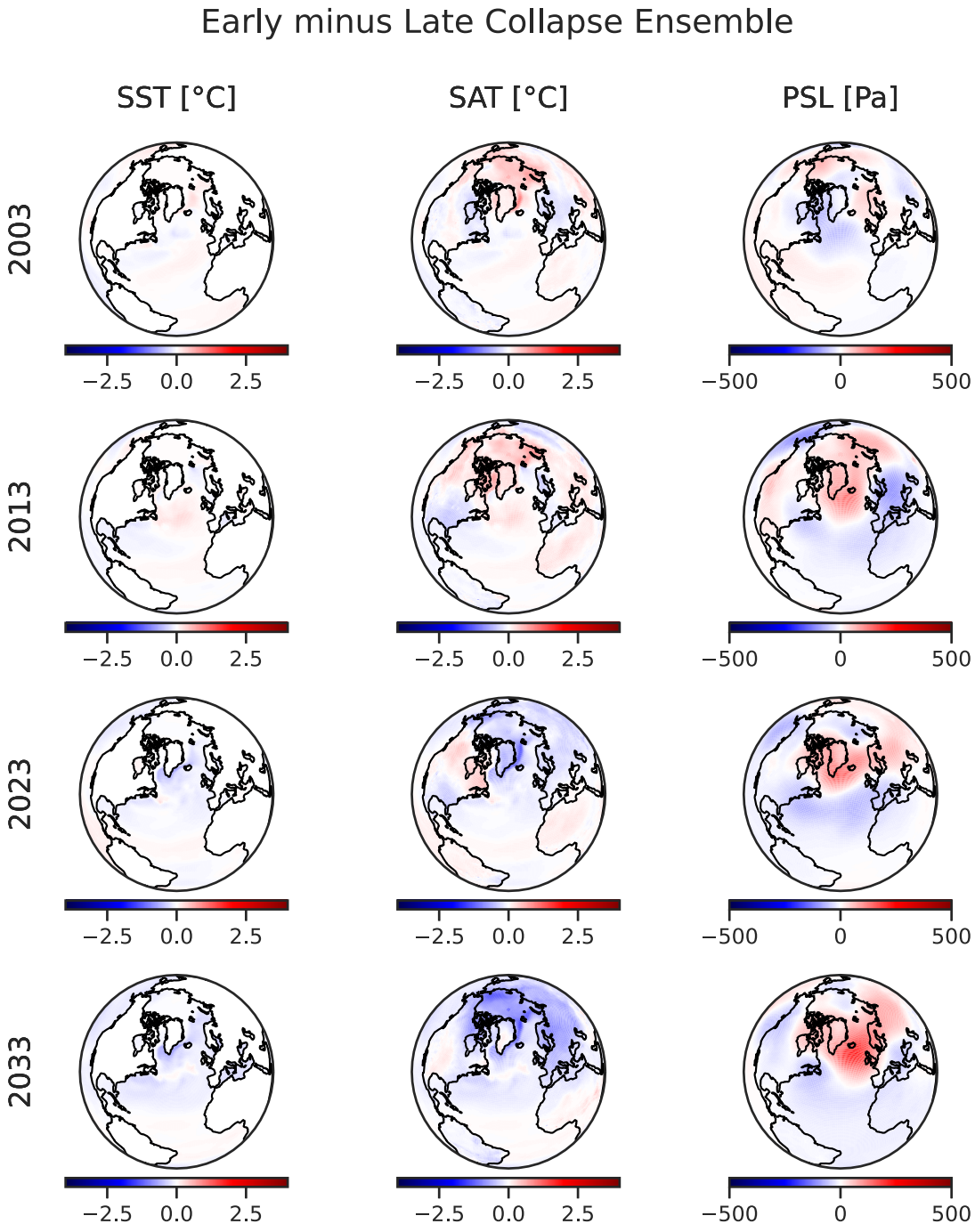

(a) First half of Figure 23. Figure continues on the next page.

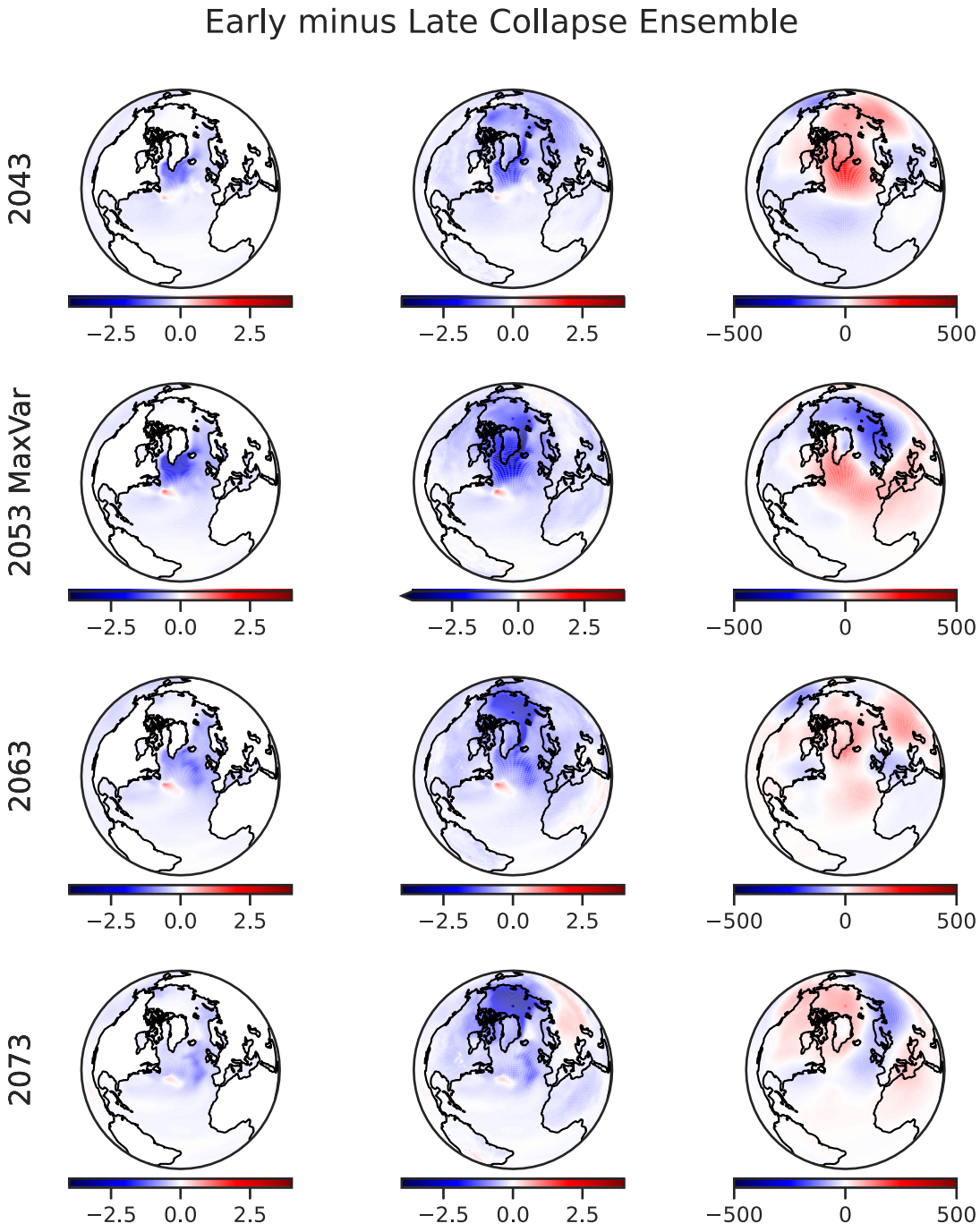

(b) Second half of Figure 23.

Figure 23: Sub Ensemble and time mean (± 5 years of indicated year) difference between the ECE and LCE (DJF season). Left column shows SST, middle column shows SAT, and right column shows PSL. The year of maximum ensemble variance in the SPG SST time series as shown in Fig.15 is indicated with "MaxVar".

Abrupt Cooling Impacts on Atmospheric Conditions

Above, we provided evidence for the PSL signal that potentially contributes to the onset of the convection collapse disappearing at the time of maximum SST difference. This made us conclude that the differences in atmospheric conditions between ECE and LCE at this point in time are likely to be caused by the cold SST anomaly. We will therefore determine differences in atmospheric conditions at this point in time to assess how abrupt cooling in the subpolar NA impacts atmospheric conditions globally.

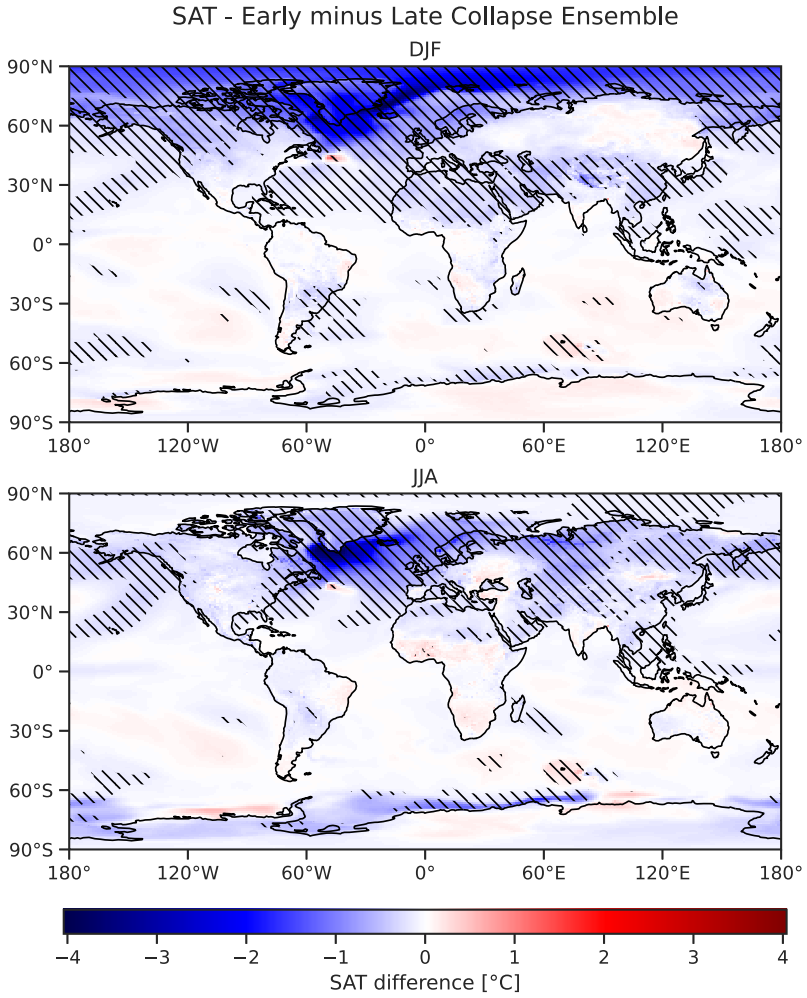

Figure 24: Ensemble and time mean (2053 ± 5 years) SAT difference between LCE and ECE in the year of maximum ensemble variance (Fig.16). Hatched area where the sub ensemble difference is significant (p-value < 0.05 ; Welch's t-test allowing for different sample variance).

Surface Air Temperature

The overall effect of abrupt cooling in the subpolar NA on the global SAT is large and we find a decrease in the annual mean SAT of $\approx 0.2°C$. In Figure 24 we observe that the cooling effect occurs almost exclusively in the NH and the SAT of the NH decreases by $\approx 0.39°C$ (annual mean). With deep convection occurring mainly in the late winter season, it is not surprising to observe that the effect of a deep convection collapse is stronger in the winter season (December to February (DJF)) compared to the summer season (June to August (JJA)). In the summer season, strong SAT cooling is mainly found in the region where we also observe the SST anomaly causing the drop in SAT. In the winter season not only the subpolar NA, but the whole Arctic region shows significant and strong cooling (SAT decrease of $\approx 2°C - 3°C$). Interestingly, contrasting the findings for the summer season, eastern Europe and Siberia show no significant SAT changes in Winter, although almost the whole NH shows significant SAT drops (Fig.24). The small but significant warming located to the south of the SPG is likely a signal that occurs due to the change in the shape of the SPG. In Figure 12 (bottom panel) we observe a strong shift in the gyre circulation. In the historical mean the corresponding region is affected by an extension of the SPG circulation. This extension vanishes and the region is now being influenced by subtropical water masses. Hence, we observe a prominent warming signal where this SPG circulation extension used to be.

Pressure at Sea Level

SLP in the direct vicinity of the cold SST anomaly increases and this response is enhanced in the NH winter season. Additionally, we identify a significant increase in SLP over North Africa and the Mediterranean and a strong decrease over the Arctic region and Scandinavia in the boreal winter season. In JJA the overall SLP response is weaker compared to DJF. The strong negative SLP difference over the Arctic disappears and we find a weak but significant positive SLP response over large parts of Eurasia.
The SLP increase over the SPG was already visible in the preceding years and could therefore be a signal of the described SLP pattern leading to the differences between ECE and LCE (see Fig.23). The strong SLP response over the Arctic, North Africa, and Mediterranean in DJF on the other hand is a strong deviation from preceding decades. Further, this SLP pattern is similar to what Swingedouw et al. (2021) identified in their model ensemble analysis as a response to abrupt cooling. Gervais et al. (2019) provide an explanation for the positive SLP signal over and downstream (eastwards) of the cold SST anomaly. They describe how a direct linear response to a cold SST anomaly results in SAT cooling over the anomaly and SLP increase downstream. We find both of these responses in Figures 24 and 25, with a more prominent signal in the NH winter season.

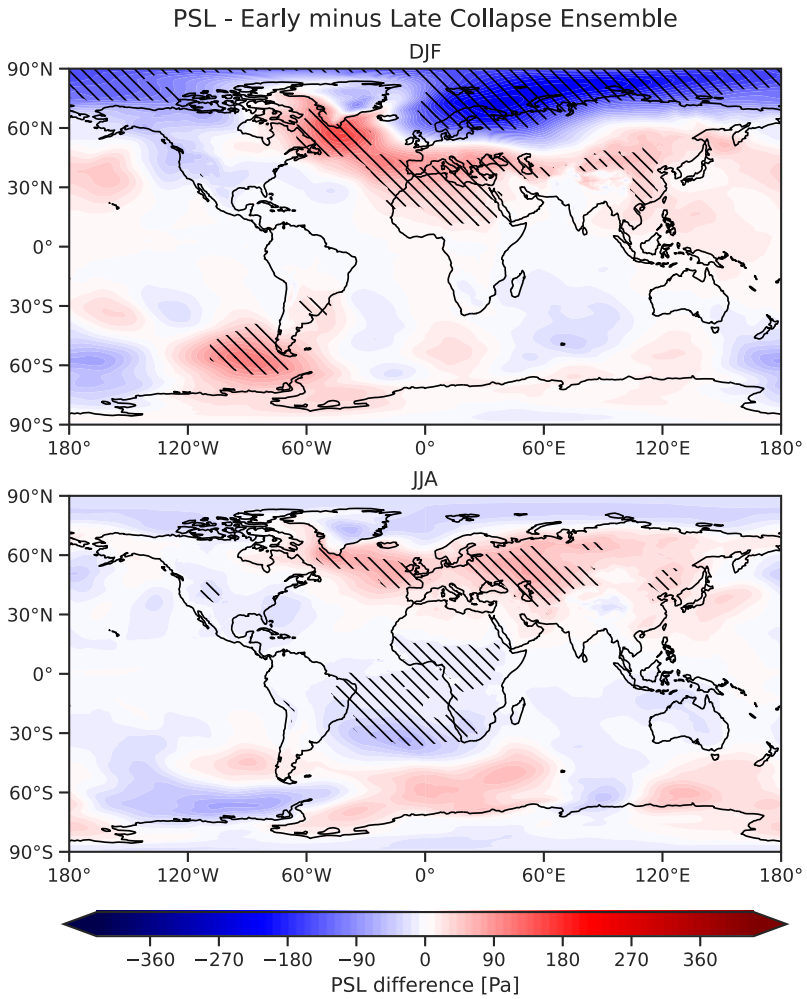

Figure 25: Ensemble and time mean (2053 ± 5 years) PSL difference between LCE and ECE in the year of maximum ensemble variance (Fig.16). Hatched area where the sub ensemble difference is significant (p-value < 0.05 ; Welch's t-test allowing for different sample variance).

Precipitation

The impact of abrupt cooling in the subpolar NA on global precipitation patterns is less prominent. In the NH winter season, we identify the strongest changes located in the SPG (Fig.26). Here, the SST anomaly is more pronounced in winter and the ocean-atmosphere temperature gradient is strongly affected in this region. Precipitation in the SPG region mostly originates from preceding evaporation in the same region. A strong decrease in ocean-atmosphere temperature gradient leads to decreased evaporation and it is therefore not surprising to find a strong decrease in precipitation in this region.
In JJA we find precipitation to decrease significantly in West Africa (Fig.26). This region

is strongly influenced by the position of the Intertropical Convergence Zone (ITCZ). Schneider et al. (2014) describe the dynamics and drivers determining the position of the ITCZ and explain how a strong AMOC helps to maintain the northward extent of the ITCZ. Sgubin et al. (2017) show that the overall changes in the atmosphere that arise from abrupt cooling in the subpolar NA are similar, but weaker in magnitude, compared to changes following a strong AMOC weakening. Described precipitation changes in Africa could therefore be a result of the ITCZ shifting southwards as a consequence of the abrupt cooling in the SPG.

One important consideration that needs to be addressed is the overall drop in the

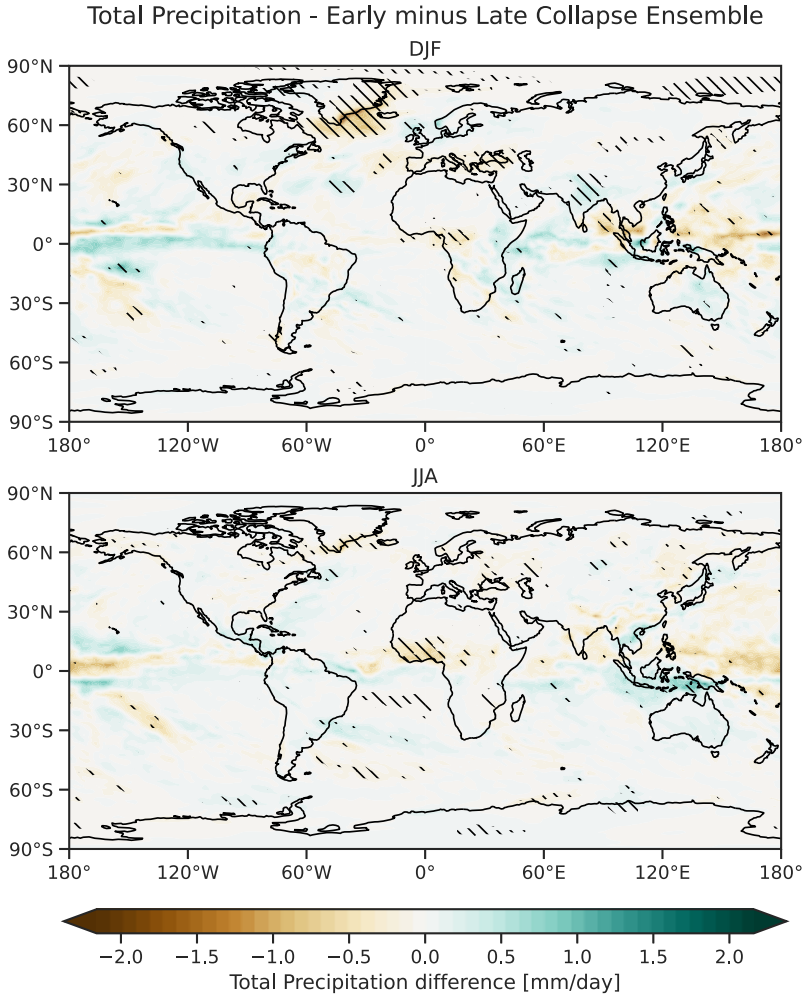

Figure 26: Ensemble and time mean (2053 $\pm$ 5 years) PRECIP difference between LCE and ECE in the year of maximum ensemble variance (Fig.16). Hatched area where the sub ensemble difference is significant (p-value < 0.05 ; Welch's t-test allowing for different sample variance).

SHF being larger than the SHF difference between the described sub ensembles in the year of maximum SST variance (2053). In Figure 21, we already observed the overall changes in the SHF towards the end of the model simulation. The SHF difference between ECE and LCE that is likely to contribute to the above-described changes in the atmospheric conditions in 2053 is approximately half of the long-term decline in the ocean-atmosphere heat loss. Therefore, the identified changes in global atmospheric conditions are likely to be stronger in magnitude than Figures 25, 24, and 26 suggest.

7 Summary and Conclusions

The overarching goal of this study was to identify the drivers of abrupt cooling events in the subpolar NA and determine how the resulting SST anomaly impacts the state of the atmosphere in CESM2. To the best of our knowledge, such an analysis using a SMILE has never been done before and we therefore provide valuable insights on the role of internal variability in convection collapse events in the subpolar NA.
We find that all ensemble members in CESM2-LENS show a collapse of deep convection and the transition towards a new stable state without active deep convection. The MLD decreases below 100 m in the annual mean in each member and does not recover from this collapsed state until the end of the model simulation. The estimated year of reaching this new state is 2058 $\pm$ 6 years. The corresponding abrupt cooling which is described to be a result of a strong decline in the MLD is estimated to happen in 2045 $\pm$ 11 years.
The collapse of deep convection occurs first in the Labrador Sea, but with a lagged response of a few decades, the whole subpolar NA shows no regions with a MLD deeper than 100 m. As a result, the SPG does not follow the positive global mean temperature trend and instead exhibits strong SST cooling of up to 4°C. The effect of this large-scale cold SST anomaly on global surface temperatures is significant. Global mean surface temperatures decrease by $\approx$ 0.2°C and Northern Hemisphere mean surface temperatures by $\approx$ 0.39°C.
We provide evidence for the surface freshening in the SPG being the cause of the negative surface density anomaly leading to deep convection collapsing. Determining two sub ensembles, representing an early and a late collapse ensemble, shows that differences in the SSS between the sub ensembles were already detectable decades prior to the final collapse. Similar early signs of differences between the early and late collapse ensembles in the MLD, AMOC, and SPG circulation strength lead to the conclusion that the actual tipping point was reached decades prior to the onset of abrupt cooling.
Studies on the SPG circulation being a tipping element with two stable states suggest the potential transition towards a weaker circulation without deep convection in the circulations center. We detect an abrupt and ongoing decline in the SPG circulation already in the historical data. Reaching the tipping point of the SPG circulation in the historical model simulation explains why we find an independence of the forcing scenario when it comes to the year in which deep convection collapses.
Additionally, we identified a consistent pattern of negative NAO-like PSL in the preceding years of convection collapse. This finding does not explain the overall SPG freshening and deep convection collapse but is likely a sign for the PSL to be a deciding factor in determining not if, but when the abrupt cooling occurs.

The collapse of deep convection in the subpolar NA is categorized to be a key tipping element of our climate system and is added to the list of tipping elements at risk

of reaching their point of no return even when keeping global mean temperatures below 1.5°C (Armstrong McKay et al., 2022). This categorization draws on the results of Sgubin et al. (2017) and Swingedouw et al. (2021). They assess the risk of abrupt cooling events in CMIP5 and CMIP6 models but do not further investigate a potential tipping point like behaviour of the SPG circulation. The estimated threshold for the SPG convection collapse from Armstrong McKay et al. (2022) indicates the point in time when deep convection collapses enough to trigger an abrupt cooling event. However, our findings suggest the actual tipping point and corresponding threshold to be reached decades prior to the abrupt cooling. The risk of triggering the described large-scale changes in the subpolar NA would therefore be underestimated and the tipping point would be reached earlier.

We have shown that using SAT instead of SST in studies investigating abrupt cooling caused by a collapse of deep convection leads to no significant changes in the results. However, we find the results to be sensitive to the choice of the reference region. From the first study on abrupt cooling events in the CMIP5 models to the second study using the CMIP6 models, Swingedouw et al. (2021) change the reference region. We provided evidence for the changes in the reference region resulting in a potential underestimation of the risk of abrupt cooling in CMIP6 models.

8 Outlook

Unveiling the mentioned misconceptions, and discovering the SPG circulations transition towards a weaker stable state without deep convection in CESM2, calls for urgent clarifications and further efforts to improve our understanding of the subpolar NA in a changing climate. Below we list the most important research questions and follow-up studies crucial for improving climate projections and correctly assessing the risk of surpassing tipping points in the real-world climate system.

- Subsequent work should be conducted to investigate if the theory of the SPG circulation being the actual tipping element holds for CESM2. It is essential to understand what leads to the abrupt and large-scale circulation changes of the SPG and the AMOC to determine where exactly the tipping point lies.
- With other models showcasing abrupt cooling events in the subpolar NA as well, it is important to study whether the corresponding drivers are similar to the ones we identify in CESM2. The main question that needs to be addressed: Are abrupt cooling events caused by a collapse of deep convection always cooccurring with large-scale SPG circulation changes?
- Our findings suggest that a potential tipping point in the subpolar NA is reached already in the historical data. Determining early warning signals is therefore essential to assess how close we are to this tipping point in the real world, or if it is already passed.
- Lastly, we hope that the above findings motivate further work aiming to improve our intuitive view of the SPG's role in the circulation of the North Atlantic. The strength and size of the SPG are often not included in conceptual studies on the potential AMOC tipping point. In turn, studies on the bistability of the SPG in simple box models do not include ice sheet meltwater or changes in the forcing from the outside in the form of AMOC variability. Our results emphasize the potential strong coupling and interplay between SPG strength and shape and the AMOC. Therefore, an innovative approach including the SPG circulation as a key element of the whole AMOC system could improve our conceptual understanding of this key element of Earth's climate system.

9 Appendix

Testing Sub Ensemble Time Series for Difference

In section 4 we determine sub ensembles consisting of 10 members each. To ascertain if the time series of these sub ensembles are significantly different, we test the two samples at each time step using Welch's t-test. Welch's t-test allows for comparing two samples with different variance. This is important due to potential strong changes in the sub ensemble variance in the proximity of the abrupt changes. To increase the sample sizes for each sub ensemble, we use a window of 11 years (plus and minus 5 years at each time step). Thus, comparing two samples of 110 values each. Using the resulting p-value time series, we can identify the point in time where a significant difference between the ETE and LTE is detectable. We focus on abrupt changes and therefore prominent events in the time series. Therefore, it is important at what time the sub ensembles diverge and proof to be significantly different until the events of interest occurred. This described point in time is marked in the corresponding plots to showcase the onset of significant difference (see Fig. 16,17).

Ensemble Variance

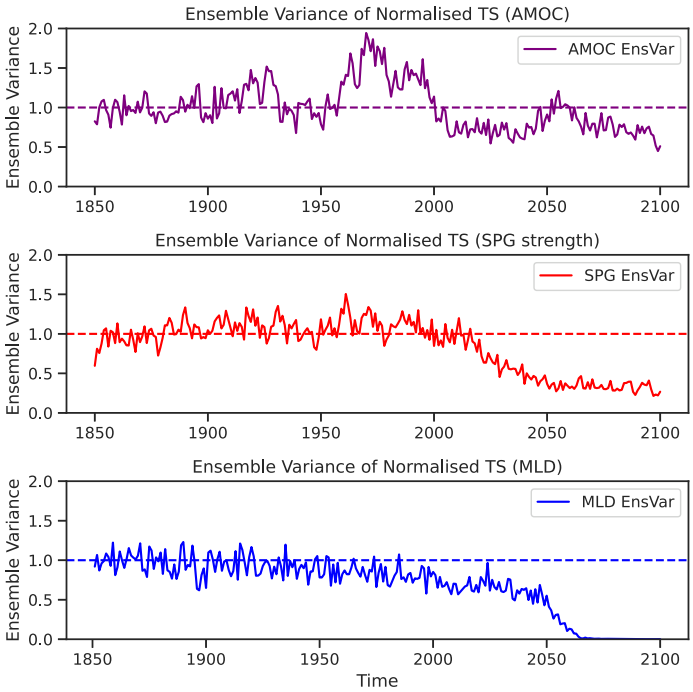

Figure 27: Ensemble variance of AMOC strength, SPG strength, and SPG MLD.

MLD and SHF correlation

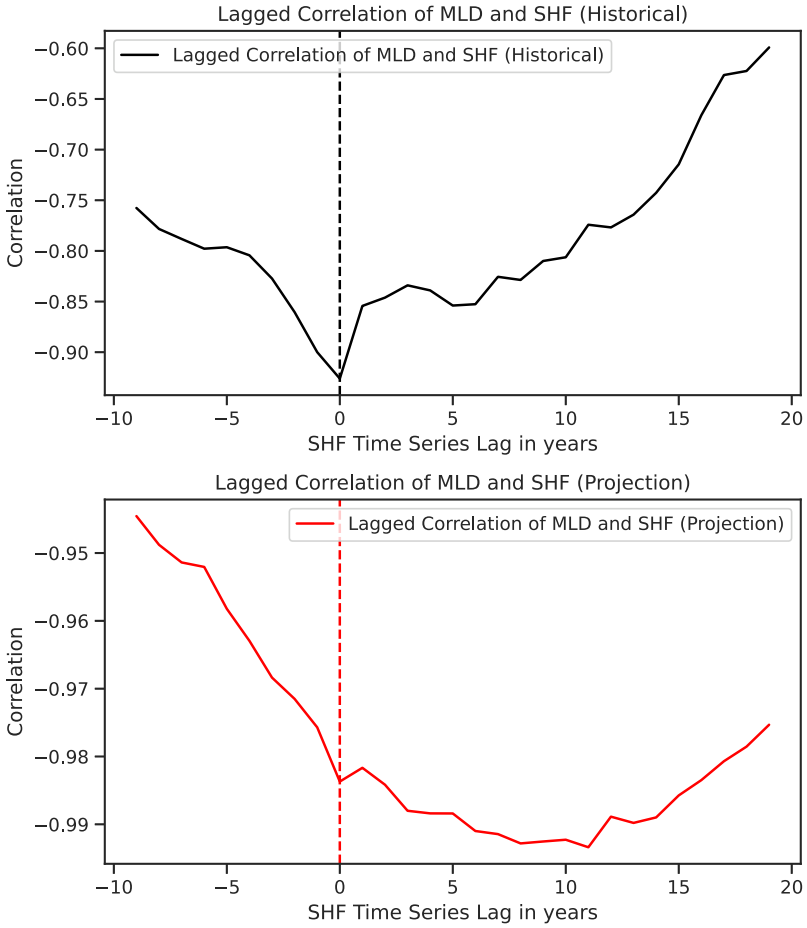

Figure 28: Correlation of the ensemble mean time series of SPG MLD and SPG SHF depending on the lag period in years. Upper panel shows lagged correlation of the historical time series from 1850 to 2015. Lower panel shows lagged correlation of the projection time series from 2015 to 2100. Vertical dashed lines indicate $lag = 0$.

10 References

Armstrong McKay, David I. et al. (Sept. 9, 2022). "Exceeding 1.5°C global warming could trigger multiple climate tipping points". In: *Science* 377.6611, eabn7950. ISSN: 0036-8075, 1095-9203. DOI: 10.1126/science.abn7950. URL: https://www.science.org/doi/10.1126/science.abn7950 (visited on 02/16/2023).

Bathiany, S., M. Scheffer, E. H. van Nes, M. S. Williamson, and T. M. Lenton (Mar. 22, 2018). "Abrupt Climate Change in an Oscillating World". In: *Scientific Reports* 8.1, p. 5040. ISSN: 2045-2322. DOI: 10.1038/s41598-018-23377-4. URL: https://www.nature.com/articles/s41598-018-23377-4 (visited on 05/06/2023).

Beckmann, Aike (2021). *Aquatic Physiosphere-Biosphere Dynamics and Modelling: A Reference for Studies of the Coupled System*. Cham: Springer International Publishing. ISBN: 978-3-030-54156-9 978-3-030-54157-6. DOI: 10.1007/978-3-030-54157-6. URL: http://link.springer.com/10.1007/978-3-030-54157-6 (visited on 03/10/2023).

Biri, Stavroula and Birgit Klein (2019). "North Atlantic Sub-Polar Gyre Climate Index: A New Approach". In: *Journal of Geophysical Research: Oceans* 124.6. ISSN: 2169-9291. DOI: 10.1029/2018JC014822. URL: https://onlinelibrary.wiley.com/doi/abs/10.1029/2018JC014822 (visited on 06/11/2023).

Boers, Niklas (Aug. 2021). "Observation-based early-warning signals for a collapse of the Atlantic Meridional Overturning Circulation". In: *Nature Climate Change* 11.8, pp. 680–688. ISSN: 1758-678X, 1758-6798. DOI: 10.1038/s41558-021-01097-4. URL: https://www.nature.com/articles/s41558-021-01097-4 (visited on 02/16/2023).

Böning, C. W., M. Scheinert, J. Dengg, A. Biastoch, and A. Funk (Sept. 29, 2006). "Decadal variability of subpolar gyre transport and its reverberation in the North Atlantic overturning". In: *Geophysical Research Letters* 33.21, L21S01. ISSN: 0094-8276. DOI: 10.1029/2006GL026906. URL: http://doi.wiley.com/10.1029/2006GL026906 (visited on 02/17/2023).

Born, A. and A. Levermann (2010). "The 8.2 ka event: Abrupt transition of the subpolar gyre toward a modern North Atlantic circulation". In: *Geochemistry, Geophysics, Geosystems* 11.6. ISSN: 1525-2027. DOI: 10.1029/2009GC003024. URL: https://onlinelibrary.wiley.com/doi/abs/10.1029/2009GC003024 (visited on 06/11/2023).

Born, Andreas and Thomas F. Stocker (Jan. 1, 2014). "Two Stable Equilibria of the Atlantic Subpolar Gyre". In: *Journal of Physical Oceanography* 44.1, pp. 246–264. ISSN: 0022-3670, 1520-0485. DOI: 10.1175/JPO-D-13-073.1. URL: https://journals.ametsoc.org/view/journals/phoc/44/1/jpo-d-13-073.1.xml (visited on 04/12/2023).

Böttinger, Michael and Dieter Kasang (2020). *The SSP Scenarios*. https://www.dkrz.de/en/communication/climate-simulations/cmip6-en/the-ssp-scenarios.

Caesar, L., S. Rahmstorf, A. Robinson, G. Feulner, and V. Saba (Apr. 2018). "Observed fingerprint of a weakening Atlantic Ocean overturning circulation". In: *Nature* 556.7700, pp. 191–196. ISSN: 0028-0836, 1476-4687. DOI: 10.1038/s41586-018-0006-5. URL: http://www.nature.com/articles/s41586-018-0006-5 (visited on 02/17/2023).

Danabasoglu, G. et al. (2020). "The Community Earth System Model Version 2 (CESM2)". In: *Journal of Advances in Modeling Earth Systems* 12.2. ISSN: 1942-2466. DOI: 10.1029/2019MS001916. URL: https://onlinelibrary.wiley.com/doi/abs/10.1029/2019MS001916 (visited on 06/03/2023).

Danabasoglu, Gokhan, Laura Landrum, Stephen G. Yeager, and Peter R. Gent (2019). "Robust and nonrobust aspects of Atlantic meridional overturning circulation variability and mechanisms in the Community Earth System Model". In: *Journal of Climate*, pp. 7349–7368. ISSN: 0894-8755. DOI: 10.1175/JCLI-D-19-0026.1. URL: https://opensky.ucar.edu/islandora/object/articles%3A22894/ (visited on 03/27/2023).

Delworth, Thomas L. and Fanrong Zeng (Feb. 1, 2016). "The Impact of the North Atlantic Oscillation on Climate through Its Influence on the Atlantic Meridional Overturning Circulation". In: *Journal of Climate* 29.3, pp. 941–962. ISSN: 0894-8755, 1520-0442. DOI: 10.1175/JCLI-D-15-0396.1. URL: http://journals.ametsoc.org/doi/10.1175/JCLI-D-15-0396.1 (visited on 03/27/2023).

Deser, C. et al. (Apr. 2020). "Insights from Earth system model initial-condition large ensembles and future prospects". In: *Nature Climate Change* 10.4, pp. 277–286. ISSN: 1758-6798. DOI: 10.1038/s41558-020-0731-2. URL: https://www.nature.com/articles/s41558-020-0731-2 (visited on 05/14/2023).

Deshayes, Julie and Claude Frankignoul (Oct. 1, 2008). "Simulated Variability of the Circulation in the North Atlantic from 1953 to 2003". In: *Journal of Climate* 21.19, pp. 4919–4933. ISSN: 0894-8755, 1520-0442. DOI: 10.1175/2008JCLI1882.1. URL: https://journals.ametsoc.org/view/journals/clim/21/19/2008jcli1882.1.xml (visited on 03/27/2023).

Drijfhout, Sybren, Geert Jan van Oldenborgh, and Andrea Cimatoribus (Dec. 15, 2012). "Is a Decline of AMOC Causing the Warming Hole above the North Atlantic in Observed and Modeled Warming Patterns?" In: *Journal of Climate* 25.24, pp. 8373–8379. ISSN: 0894-8755, 1520-0442. DOI: 10.1175/JCLI-D-12-00490.1. URL: https://journals.ametsoc.org/view/journals/clim/25/24/jcli-d-12-00490.1.xml (visited on 04/22/2023).

Duchez, Aurélie et al. (July 1, 2016). "Drivers of exceptionally cold North Atlantic Ocean temperatures and their link to the 2015 European heat wave". In: *Environmental Research Letters* 11.7, p. 074004. ISSN: 1748-9326. DOI: 10.1088/1748-9326/11/7/074004. URL: https://iopscience.iop.org/article/10.1088/1748-9326/11/7/074004 (visited on 02/16/2023).

Foukal, Nicholas P. and M. Susan Lozier (Aug. 2017). "Assessing variability in the size and strength of the ¡span style="font-variant:small-caps;"¿N¡/span¿ orth ¡span

style=" font-variant:small-caps;" ¿A¡/span¿ tlantic subpolar gyre". In: *Journal of Geophysical Research: Oceans* 122.8, pp. 6295–6308. ISSN: 2169-9275, 2169-9291. DOI: 10.1002/2017JC012798. URL: https://onlinelibrary.wiley.com/doi/10.1002/2017JC012798 (visited on 02/17/2023).

Gervais, Melissa, Jeffrey Shaman, and Yochanan Kushnir (May 15, 2019). "Impacts of the North Atlantic Warming Hole in Future Climate Projections: Mean Atmospheric Circulation and the North Atlantic Jet". In: *Journal of Climate* 32.10, pp. 2673–2689. ISSN: 0894-8755, 1520-0442. DOI: 10.1175/JCLI-D-18-0647.1. URL: https://journals.ametsoc.org/view/journals/clim/32/10/jcli-d-18-0647.1.xml (visited on 02/16/2023).

Ghosh, Rohit, Wolfgang A. Müller, Astrid Eichhorn, Johanna Baehr, and Jürgen Bader (July 2019). "Atmospheric pathway between Atlantic multidecadal variability and European summer temperature in the atmospheric general circulation model ECHAM6". In: *Climate Dynamics* 53.1, pp. 209–224. ISSN: 0930-7575, 1432-0894. DOI: 10.1007/s00382-018-4578-4. URL: http://link.springer.com/10.1007/s00382-018-4578-4 (visited on 02/16/2023).

Ghosh, Rohit, Dian Putrasahan, Elisa Manzini, Katja Lohmann, Paul Keil, Ralf Hand, Jürgen Bader, Daniela Matei, and Johann H. Jungclaus (Feb. 23, 2023). "Two Distinct Phases of North Atlantic Eastern Subpolar Gyre and Warming Hole Evolution under Global Warming". In: *Journal of Climate* 36.6, pp. 1881–1894. ISSN: 0894-8755, 1520-0442. DOI: 10.1175/JCLI-D-22-0222.1. URL: https://journals.ametsoc.org/view/journals/clim/36/6/JCLI-D-22-0222.1.xml (visited on 03/29/2023).

Hand, Ralf (2020). "Changes of Decadal SST Variations in the Subpolar North Atlantic under Strong CO2 Forcing as an Indicator for the Ocean Circulation's Contribution to Atlantic Multidecadal Variability". In: *JOURNAL OF CLIMATE* 33.

Koul, Vimal, Jan-Erik Tesdal, Manfred Bersch, Hjálmar Hátún, Sebastian Brune, Leonard Borchert, Helmuth Haak, Corinna Schrum, and Johanna Baehr (Jan. 22, 2020). "Unraveling the choice of the north Atlantic subpolar gyre index". In: *Scientific Reports* 10.1, p. 1005. ISSN: 2045-2322. DOI: 10.1038/s41598-020-57790-5. URL: https://www.nature.com/articles/s41598-020-57790-5 (visited on 05/07/2023).

Lenton, Timothy M. (July 2011). "Early warning of climate tipping points". In: *Nature Climate Change* 1.4, pp. 201–209. ISSN: 1758-6798. DOI: 10.1038/nclimate1143. URL: https://www.nature.com/articles/nclimate1143 (visited on 05/16/2023).

– (Feb. 2012). "Arctic Climate Tipping Points". In: *AMBIO* 41.1, pp. 10–22. ISSN: 0044-7447, 1654-7209. DOI: 10.1007/s13280-011-0221-x. URL: http://link.springer.com/10.1007/s13280-011-0221-x (visited on 02/16/2023).

Lenton, Timothy M., Hermann Held, Elmar Kriegler, Jim W. Hall, Wolfgang Lucht, Stefan Rahmstorf, and Hans Joachim Schellnhuber (Feb. 12, 2008). "Tipping elements in the Earth's climate system". In: *Proceedings of the National Academy of Sciences*

105.6, pp. 1786–1793. DOI: 10.1073/pnas.0705414105. URL: https://www.pnas.org/doi/abs/10.1073/pnas.0705414105 (visited on 05/11/2023).

Levitus, Sydney et al. (2012). "World ocean heat content and thermosteric sea level change (0–2000 m), 1955–2010". In: *Geophysical Research Letters* 39.10.

Liu, Teng et al. (Jan. 2023). "Teleconnections among tipping elements in the Earth system". In: *Nature Climate Change* 13.1, pp. 67–74. ISSN: 1758-678X, 1758-6798. DOI: 10.1038/s41558-022-01558-4. URL: https://www.nature.com/articles/s41558-022-01558-4 (visited on 03/25/2023).

Liu, Wei, Shang-Ping Xie, Zhengyu Liu, and Jiang Zhu (Jan. 6, 2017). "Overlooked possibility of a collapsed Atlantic Meridional Overturning Circulation in warming climate". In: *Science Advances* 3.1, e1601666. ISSN: 2375-2548. DOI: 10.1126/sciadv.1601666. URL: https://www.science.org/doi/10.1126/sciadv.1601666 (visited on 02/16/2023).

Lohmann, Katja, Helge Drange, and Mats Bentsen (2009a). "A possible mechanism for the strong weakening of the North Atlantic subpolar gyre in the mid-1990s". In: *Geophysical Research Letters* 36.15. ISSN: 1944-8007. DOI: 10.1029/2009GL039166. URL: https://onlinelibrary.wiley.com/doi/abs/10.1029/2009GL039166 (visited on 03/27/2023).

– (Feb. 2009b). "Response of the North Atlantic subpolar gyre to persistent North Atlantic oscillation like forcing". In: *Climate Dynamics* 32.2, pp. 273–285. ISSN: 0930-7575, 1432-0894. DOI: 10.1007/s00382-008-0467-6. URL: http://link.springer.com/10.1007/s00382-008-0467-6 (visited on 02/17/2023).

Lontzek, Thomas S., Yongyang Cai, Kenneth L. Judd, and Timothy M. Lenton (May 2015). "Stochastic integrated assessment of climate tipping points indicates the need for strict climate policy". In: *Nature Climate Change* 5.5, pp. 441–444. ISSN: 1758-6798. DOI: 10.1038/nclimate2570. URL: https://www.nature.com/articles/nclimate2570 (visited on 05/09/2023).

Lozier, M. S. et al. (Feb. 2019). "A sea change in our view of overturning in the subpolar North Atlantic". In: *Science* 363.6426, pp. 516–521. ISSN: 0036-8075, 1095-9203. DOI: 10.1126/science.aau6592. URL: https://www.science.org/doi/10.1126/science.aau6592 (visited on 02/17/2023).

Maher, Nicola, Sebastian Milinski, and Ralf Ludwig (Apr. 22, 2021). "Large ensemble climate model simulations: introduction, overview, and future prospects for utilising multiple types of large ensemble". In: *Earth System Dynamics* 12.2, pp. 401–418. ISSN: 2190-4987. DOI: 10.5194/esd-12-401-2021. URL: https://esd.copernicus.org/articles/12/401/2021/ (visited on 02/16/2023).

Meinshausen, Malte et al. (Aug. 13, 2020). "The shared socio-economic pathway (SSP) greenhouse gas concentrations and their extensions to 2500". In: *Geoscientific Model Development* 13.8, pp. 3571–3605. ISSN: 1991-959X. DOI: 10.5194/gmd-13-3571-2020. URL: https://gmd.copernicus.org/articles/13/3571/2020/ (visited on 05/14/2023).

Menary, Matthew B. and Richard A. Wood (Apr. 1, 2018). "An anatomy of the projected North Atlantic warming hole in CMIP5 models". In: *Climate Dynamics* 50.7, pp. 3063–3080. ISSN: 1432-0894. DOI: 10.1007/s00382-017-3793-8. URL: https://doi.org/10.1007/s00382-017-3793-8 (visited on 06/22/2023).

Paris Agreement (2019). URL: https://treaties.un.org/pages/ViewDetails.aspx?src=TREATY&mtdsg_no=XXVII-7-d&chapter=27&clang=_en (visited on 03/28/2019).

Rodgers, Keith B. et al. (Dec. 9, 2021). "Ubiquity of human-induced changes in climate variability". In: *Earth System Dynamics* 12.4, pp. 1393–1411. ISSN: 2190-4979. DOI: 10.5194/esd-12-1393-2021. URL: https://esd.copernicus.org/articles/12/1393/2021/ (visited on 05/14/2023).

Roquet, Fabien and Carl Wunsch (Nov. 7, 2022). "The Atlantic Meridional Overturning Circulation and its Hypothetical Collapse". In: *Tellus A: Dynamic Meteorology and Oceanography* 74.1, pp. 393–398. ISSN: 1600-0870. DOI: 10.16993/tellusa.679. URL: https://a.tellusjournals.se/articles/10.16993/tellusa.679/ (visited on 02/17/2023).

Schneider, Tapio, Tobias Bischoff, and Gerald H. Haug (Sept. 2014). "Migrations and dynamics of the intertropical convergence zone". In: *Nature* 513.7516, pp. 45–53. ISSN: 1476-4687. DOI: 10.1038/nature13636. URL: https://www.nature.com/articles/nature13636 (visited on 06/16/2023).

Sgubin, Giovanni, Didier Swingedouw, Sybren Drijfhout, Yannick Mary, and Amine Bennabi (Feb. 15, 2017). "Abrupt cooling over the North Atlantic in modern climate models". In: *Nature Communications* 8.1, p. 14375. ISSN: 2041-1723. DOI: 10.1038/ncomms14375. URL: https://www.nature.com/articles/ncomms14375 (visited on 02/16/2023).

Smith, R et al. (2010). "The parallel ocean program (POP) reference manual ocean component of the community climate system model (CCSM) and community earth system model (CESM)". In: *LAUR-01853* 141, pp. 1–140.

Steffen, Will et al. (Aug. 14, 2018). "Trajectories of the Earth System in the Anthropocene". In: *Proceedings of the National Academy of Sciences* 115.33, pp. 8252–8259. ISSN: 0027-8424, 1091-6490. DOI: 10.1073/pnas.1810141115. URL: https://pnas.org/doi/full/10.1073/pnas.1810141115 (visited on 02/16/2023).

Swingedouw, Didier, Adrien Bily, Claire Esquerdo, Leonard F. Borchert, Giovanni Sgubin, Juliette Mignot, and Matthew Menary (Nov. 2021). "On the risk of abrupt changes in the North Atlantic subpolar gyre in CMIP6 models". In: *Annals of the New York Academy of Sciences* 1504.1, pp. 187–201. ISSN: 0077-8923, 1749-6632. DOI: 10.1111/nyas.14659. URL: https://onlinelibrary.wiley.com/doi/10.1111/nyas.14659 (visited on 02/16/2023).

Swingedouw, Didier, Marie-Noëlle Houssais, Christophe Herbaut, Anne-Cecile Blaizot, Marion Devilliers, and Julie Deshayes (2022). "AMOC Recent and Future Trends: A Crucial Role for Oceanic Resolution and Greenland Melting?" In: *Frontiers in Climate*

4. ISSN: 2624-9553. URL: https://www.frontiersin.org/articles/10.3389/fclim.2022.838310 (visited on 05/07/2023).

Swingedouw, Didier, Chinwe Ifejika Speranza, Annett Bartsch, Gael Durand, Cedric Jamet, Gregory Beaugrand, and Alessandra Conversi (Nov. 2020). "Early Warning from Space for a Few Key Tipping Points in Physical, Biological, and Social-Ecological Systems". In: *Surveys in Geophysics* 41.6, pp. 1237–1284. ISSN: 0169-3298, 1573-0956. DOI: 10.1007/s10712-020-09604-6. URL: https://link.springer.com/10.1007/s10712-020-09604-6 (visited on 02/16/2023).

Thornalley, David J. R. et al. (Apr. 2018). "Anomalously weak Labrador Sea convection and Atlantic overturning during the past 150 years". In: *Nature* 556.7700, pp. 227–230. ISSN: 0028-0836, 1476-4687. DOI: 10.1038/s41586-018-0007-4. URL: http://www.nature.com/articles/s41586-018-0007-4 (visited on 02/17/2023).

Ting, Mingfang, Yochanan Kushnir, Richard Seager, and Cuihua Li (2009). "Forced and internal twentieth-century SST trends in the North Atlantic". In: *Journal of Climate* 22.6, pp. 1469–1481.

Wanner, Heinz, Stefan Brönnimann, Carlo Casty, Dimitrios Gyalistras, Jürg Luterbacher, Christoph Schmutz, David B. Stephenson, and Eleni Xoplaki (July 1, 2001). "North Atlantic Oscillation – Concepts And Studies". In: *Surveys in Geophysics* 22.4, pp. 321–381. ISSN: 1573-0956. DOI: 10.1023/A:1014217317898. URL: https://doi.org/10.1023/A:1014217317898 (visited on 06/15/2023).

Wunderling, Nico, Ricarda Winkelmann, Johan Rockström, Sina Loriani, David I. Armstrong McKay, Paul D. L. Ritchie, Boris Sakschewski, and Jonathan F. Donges (Jan. 2023). "Global warming overshoots increase risks of climate tipping cascades in a network model". In: *Nature Climate Change* 13.1, pp. 75–82. ISSN: 1758-6798. DOI: 10.1038/s41558-022-01545-9. URL: https://www.nature.com/articles/s41558-022-01545-9 (visited on 03/30/2023).

Yeager, Stephen (Oct. 1, 2020). "The abyssal origins of North Atlantic decadal predictability". In: *Climate Dynamics* 55.7, pp. 2253–2271. ISSN: 1432-0894. DOI: 10.1007/s00382-020-05382-4. URL: https://doi.org/10.1007/s00382-020-05382-4 (visited on 04/04/2023).

Yeager, Stephen and Gokhan Danabasoglu (May 1, 2014). "The Origins of Late-Twentieth-Century Variations in the Large-Scale North Atlantic Circulation". In: *Journal of Climate* 27.9, pp. 3222–3247. ISSN: 0894-8755, 1520-0442. DOI: 10.1175/JCLI-D-13-00125.1. URL: https://journals.ametsoc.org/view/journals/clim/27/9/jcli-d-13-00125.1.xml (visited on 05/07/2023).

Zhang, Rong, Rowan Sutton, Gokhan Danabasoglu, Thomas L. Delworth, Who M. Kim, Jon Robson, and Stephen G. Yeager (June 24, 2016). "Comment on "The Atlantic Multidecadal Oscillation without a role for ocean circulation"". In: *Science* 352.6293, pp. 1527–1527. DOI: 10.1126/science.aaf1660. URL: https://www.science.org/doi/full/10.1126/science.aaf1660 (visited on 05/09/2023).